

Initial conditions for Inflation in an FRW Universe

Swagat S. Mishra,^a Varun Sahni^a and Alexey V. Toporensky^{b,c}

^aInter-University Centre for Astronomy and Astrophysics, Post Bag 4, Ganeshkhind, Pune 411 007, India

^bSternberg Astronomical Institute, Moscow State University, Universitetsky Prospekt, 13, Moscow 119992, Russia

^cKazan Federal University, Kremlevskaya 18, Kazan, 420008, Russia

E-mail: swagat@iucaa.in, varun@iucaa.in, atopor@rambler.ru

Abstract. We examine the class of initial conditions which give rise to inflation. Our analysis is carried out for several popular models including: Higgs inflation, Starobinsky inflation, chaotic inflation, axion monodromy inflation and non-canonical inflation. In each case we determine the set of initial conditions which give rise to sufficient inflation, with at least 60 e-foldings. A phase-space analysis has been performed for each of these models and the effect of the initial inflationary energy scale on inflation has been studied numerically. This paper discusses two scenarios of Higgs inflation: (i) the Higgs is coupled to the scalar curvature, (ii) the Higgs Lagrangian contains a non-canonical kinetic term. In both cases we find Higgs inflation to be very robust since it can arise for a large class of initial conditions. One of the central results of our analysis is that, for plateau-like potentials associated with the Higgs and Starobinsky models, inflation can be realized even for initial scalar field values which lie close to the *minimum* of the potential. This dispels a misconception relating to plateau potentials prevailing in the literature. We also find that inflation in all models is more robust for larger values of the initial energy scale.

Keywords: Inflation

Contents

1	Introduction	1
2	Methodology	2
3	Inflation with Power-law Potentials	4
3.1	Chaotic Inflation	4
3.2	Monodromy Inflation	6
3.3	Comparison of power law potentials	10
4	Higgs Inflation	13
4.1	Initial conditions for Higgs Inflation in the non-minimal framework	15
4.2	Initial conditions for Higgs Inflation in the non-canonical framework	24
5	Starobinsky Inflation	30
5.1	Action and Potential in the Einstein Frame	30
5.2	Generality of Starobinsky Inflation	34
6	Discussion	36
7	Acknowledgements	39
A	The values of n_s and r for several inflationary models	39
B	Jordan to Einstein frame transformation for Higgs inflation	40
C	Derivation of asymptotic forms of the Higgs potential in the Einstein frame	42

1 Introduction

Since its inception in the early 1980's, the inflationary scenario has emerged as a popular paradigm for describing the physics of the very early universe [1–5]. A major reason for the success of the inflationary scenario is that, in tandem with explaining many observational features of our universe – including its homogeneity, isotropy and spatial flatness, it can also account for the existence of galaxies, via the mechanism of tiny initial (quantum) fluctuations which are subsequently amplified through gravitational instability [6–9].

An important issue that needs to be addressed by a successful model of inflation is whether the universe can inflate starting from a sufficiently large class of initial conditions. This issue was affirmatively answered for chaotic inflation in the early papers [10, 11]. Since then the inventory of inflationary models has rapidly increased. In this paper we attempt to generalize the analysis of [10, 11] to other popular inflationary models including Higgs inflation, Starobinsky inflation etc., emphasising the distinction between power law potentials and asymptotically flat ‘plateau-like’ potentials. As we shall show, our results for asymptotically flat potentials do not provide support to the ‘*unlikeliness problem*’ raised in [12]¹.

¹See [13] for an analysis of other problems with plateau-like potentials raised in [12].

Our paper is organized as follows. We introduce our method of analysis in section 2. Section 3 discusses power law potentials and includes chaotic inflation and monodromy inflation. Section 4 discusses Higgs inflation in the context of both the non-minimal as well as the non-canonical framework². Section 5 is devoted to Starobinsky inflation. Our results are presented in section 6.

We work in the units $c, \hbar = 1$ and the reduced Planck mass is assumed to be $m_p = \frac{1}{\sqrt{8\pi G}}$. The metric signature is $(-, +, +, +)$. For simplicity we assume that the pre-inflationary patch which resulted in inflation was homogeneous, isotropic and spatially flat. An examination of inflation within a more general cosmological setting can be found in [15].

2 Methodology

The action for a scalar field which couples minimally to gravity has the following general form

$$S[\phi] = \int d^4x \sqrt{-g} \mathcal{L}(F, \phi), \quad (2.1)$$

where the Lagrangian density $\mathcal{L}(\phi, F)$ is a function of the field ϕ and the kinetic term

$$F = \frac{1}{2} \partial_\mu \phi \partial^\mu \phi. \quad (2.2)$$

Varying (2.1) with respect to ϕ results in the equation of motion

$$\frac{\partial \mathcal{L}}{\partial \phi} - \left(\frac{1}{\sqrt{-g}} \right) \partial_\mu \left(\sqrt{-g} \frac{\partial \mathcal{L}}{\partial (\partial_\mu \phi)} \right) = 0. \quad (2.3)$$

The energy-momentum tensor associated with the scalar field is

$$T^{\mu\nu} = \left(\frac{\partial \mathcal{L}}{\partial F} \right) (\partial^\mu \phi \partial^\nu \phi) - g^{\mu\nu} \mathcal{L}. \quad (2.4)$$

Specializing to a spatially flat FRW universe and a homogeneous scalar field, one gets

$$ds^2 = -dt^2 + a^2(t) [dx^2 + dy^2 + dz^2], \quad (2.5)$$

$$T^\mu{}_\nu = \text{diag}(-\rho_\phi, p_\phi, p_\phi, p_\phi), \quad (2.6)$$

where the energy density, ρ_ϕ , and pressure, p_ϕ , are given by

$$\rho_\phi = \left(\frac{\partial \mathcal{L}}{\partial F} \right) (2F) - \mathcal{L}, \quad (2.7)$$

$$p_\phi = \mathcal{L}, \quad (2.8)$$

and $F = -(\dot{\phi}^2/2)$. The evolution of the scale factor $a(t)$ is governed by the Friedmann equations:

$$\left(\frac{\dot{a}}{a} \right)^2 = \left(\frac{8\pi G}{3} \right) \rho_\phi, \quad (2.9)$$

$$\frac{\ddot{a}}{a} = - \left(\frac{4\pi G}{3} \right) (\rho_\phi + 3p_\phi), \quad (2.10)$$

²As pointed out in [14] non-canonical scalars permit the Higgs field to play the role of the inflaton.

where ρ_ϕ satisfies the conservation equation

$$\dot{\rho}_\phi = -3H(\rho_\phi + p_\phi), \quad H \equiv \frac{\dot{a}}{a}. \quad (2.11)$$

For a canonical scalar field

$$\mathcal{L}(F, \phi) = -F - V(\phi), \quad (2.12)$$

Substituting (2.12) into (2.7) and (2.8), we find

$$\begin{aligned} \rho_\phi &= \frac{1}{2}\dot{\phi}^2 + V(\phi), \\ p_\phi &= \frac{1}{2}\dot{\phi}^2 - V(\phi), \end{aligned} \quad (2.13)$$

consequently the two Friedmann equations (2.9) and (2.10) become

$$H^2 = \frac{8\pi G}{3} \left[\frac{1}{2}\dot{\phi}^2 + V(\phi) \right], \quad (2.14)$$

$$\frac{\ddot{a}}{a} = -\frac{8\pi G}{3} \left[\dot{\phi}^2 - V(\phi) \right]. \quad (2.15)$$

Noting that $\dot{H} + H^2 = \ddot{a}/a$ one finds $\dot{H} = -4\pi G\dot{\phi}^2 < 0$, which informs us that the expansion rate is a monotonically decreasing function of time for canonical scalar fields which couple minimally to gravity. The scalar field equation of motion follows from (2.3)

$$\ddot{\phi} + 3H\dot{\phi} + V'(\phi) = 0. \quad (2.16)$$

Within the context of inflation, a scalar field rolling down its potential is usually associated with the Hubble slow roll parameters [5]

$$\epsilon_H = 2m_p^2 \left(\frac{H'(\phi)}{H(\phi)} \right)^2, \quad \eta_H = 2m_p^2 \frac{H''(\phi)}{H(\phi)} \quad (2.17)$$

and the potential slow-roll parameters [5]

$$\epsilon = \frac{m_p^2}{2} \left(\frac{V'}{V} \right)^2, \quad \eta = m_p^2 \frac{V''}{V}. \quad (2.18)$$

For small values of these parameters $\epsilon_H \ll 1, \eta_H \ll 1$, one finds $\epsilon_H \simeq \epsilon$ and $\eta_H \simeq \eta - \epsilon$. The expression for ϵ_H in (2.17) can be rewritten as $\epsilon_H = -\frac{\dot{H}}{H^2}$ which implies that the universe accelerates, $\ddot{a} > 0$, when $\epsilon_H < 1$. For the scalar field models discussed in this paper $\dot{H} = -4\pi G\dot{\phi}^2$ so that $\epsilon_H = 4\pi G\dot{\phi}^2/H^2$, which reduces to $\epsilon_H \simeq \frac{3}{2}\dot{\phi}^2/V$ when $\dot{\phi}^2 \ll V$.

The slow-roll parameters play an important role in determining the spectral index of scalar perturbations, since³, $n_s - 1 = -6\epsilon + 2\eta$. Observations indicate [16] $n_s \simeq 0.97$ which suggests that $\epsilon, \eta \ll 1$ on scales associated with the present cosmological horizon. The fact that ϵ, η are required to be rather small might appear to imply that successful inflation can only arise under a very restricted set of initial conditions, namely those for which $\dot{\phi}^2/V(\phi) \ll 1$. This need not necessarily be the case. As originally demonstrated in the context of chaotic inflation [10, 11], a scalar field rolling down a power law potential can

³Here $n_s - 1 \equiv \frac{d \ln \mathcal{P}_s}{d \ln k}$, where \mathcal{P}_s is the power spectrum of scalar curvature perturbations.

arrive at the attractor trajectory $\epsilon, \eta \ll 1$ from a very wide range of initial conditions. In this paper we shall apply the methods developed in [10, 11, 17] to several inflationary models with power law and plateau-like potentials in order to assess the impact of initial conditions on these models.

In addition to the field equations developed earlier, we shall find it convenient to work with the parameter

$$N_e = \log \frac{a(t_{\text{end}})}{a(t_{\text{initial}})} = \int_{t_i}^{t_e} H dt \equiv - \int_{\phi_e}^{\phi} \left(\frac{H}{\dot{\phi}} \right) d\phi \quad (2.19)$$

which describes the number of inflationary e-foldings since the onset of inflation. For our purpose it will also be instructive to rewrite the Friedman equation (2.14) as

$$R^2 = X^2 + Y^2 \quad (2.20)$$

where

$$R = \sqrt{6} \frac{H}{m_p}, \quad X = \hat{\phi} \frac{\sqrt{2V(\phi)}}{m_p^2}, \quad Y = \frac{1}{m_p^2} \frac{d\phi}{dt}, \quad (2.21)$$

where $\hat{\phi} = \frac{\phi}{|\phi|}$ is the sign of ϕ (this definition ensures that X and ϕ have the same sign). Clearly, holding R fixed and varying X and Y , one arrives at a set of initial conditions which satisfy the constraint equation (2.20) defining the boundary of a circle of radius R . Adequate inflation is then qualified by the range of initial values of X and Y for which the universe inflates by at least 60 e-foldings, *i.e.* $N_e \geq 60$.

We commence our discussion of inflationary models by an analysis of power law potentials which are usually associated with Chaotic inflation [11, 18].

3 Inflation with Power-law Potentials

3.1 Chaotic Inflation

We first consider the potential [18]

$$V(\phi) = \frac{1}{2} m^2 \phi^2 \quad (3.1)$$

where $m \simeq 5.97 \times 10^{-6} m_p$ is assumed, in agreement with observations of the cosmic microwave background [16, 19] (see Appendix A). The generality of this model is studied by plotting the phase-space diagram (Y vs X) and determining the region of initial conditions which gives rise to $N_e \geq 60$. Equations (2.15), (2.16), (2.19) have been solved numerically for different initial energy scales H_i . The phase-space diagram corresponding to $H_i = 3 \times 10^{-3} m_p$ is shown in figure 1.

To study the effect of different energy scales on inflation, we take different values of R ($\equiv \sqrt{6} H_i / m_p$) and determine the range of initial values of ϕ that lead to adequate inflation with $N_e \geq 60$. (The initial value of $\dot{\phi}$ is conveniently determined from the consistency relation (2.20).) Our results are summarized in figure 3. The solid blue lines correspond to initial values, ϕ_i , which always result in adequate inflation (irrespective of the sign of $\dot{\phi}_i$). The dashed red lines corresponding to $\phi_i \in [-\phi_B, -\phi_A] \cup [\phi_A, \phi_B]$, result in adequate inflation only when $\dot{\phi}_i$ points in the direction of increasing $V(\phi)$ (represented by blue arrows). Inadequate inflation is associated with the region $\phi_i \in [-\phi_A, \phi_A]$. If the initial scalar field

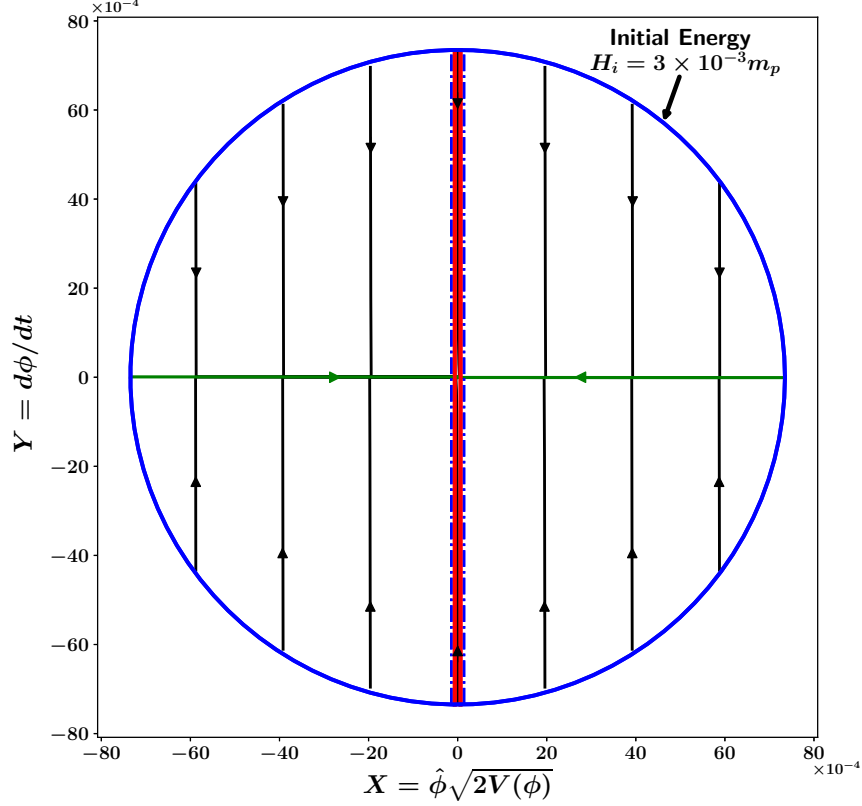


Figure 1: This figure illustrates the phase-space of chaotic inflation described by the potential (3.1). Y ($= \dot{\phi}$) is plotted against X ($= \hat{\phi}\sqrt{2V(\phi)}$) for different initial conditions all of which commence on the circumference of a circle (blue) with radius $R = \sqrt{6}H_i/m_p$ corresponding to the initial energy scale $H_i = 3 \times 10^{-3}m_p$. ($\hat{\phi} = \frac{\phi}{|\phi|}$ is the sign of field ϕ .) One finds that commencing from the circle, the different inflationary trajectories rapidly converge towards one of the two inflationary separatrices (green horizontal lines). After this, the scalar field moves towards the minimum of the potential $V(\phi)$ at $X = 0, Y = 0$. The thin vertical central band (red) corresponds to the region in phase-space that *does not* lead to adequate inflation ($N_e < 60$). This central region is shown greatly magnified in figure 2.

value falls within this region then one does not get adequate inflation *irrespective of the sign* of $\dot{\phi}_i$. This region is shown in figure 3 by the solid red line. The dependence of ϕ_A and ϕ_B on the initial energy scale H_i is given in table 1.

To determine the fraction of initial conditions that do not lead to adequate inflation (we call this ‘the degree of inadequate inflation’), we consider a uniform measure on the distribution of initial conditions for $Y_i (\equiv \dot{\phi}_i)$ and $X_i (\equiv \hat{\phi}_i \sqrt{2V(\phi_i)})$. These initial conditions are described by a circle of circumference $l = 2\pi R$ with $R = \sqrt{6}H_i$ (in Planck units) which is illustrated in figure 4. The degree of inadequate inflation and marginally adequate inflation (corresponding respectively to ϕ_A and ϕ_B in figure 3) is $2\frac{\Delta l_A}{l}$ and $2\frac{\Delta l_B}{l}$, where Δl_A and Δl_B

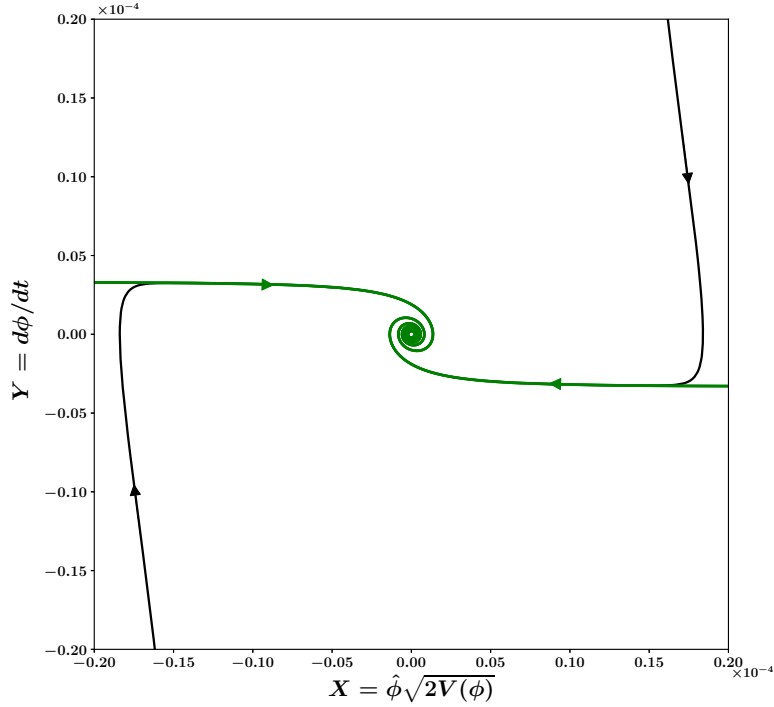


Figure 2: A zoomed-in view of the central region of figure 1. Note that $\hat{\phi} = \frac{\phi}{|\phi|}$ gives the sign of ϕ . Inflationary trajectories (black) corresponding to different initial values of ϕ and $\dot{\phi}$, first converge onto the slow-roll inflationary separatrices (green horizontal lines) before winding up to spiral towards the center.

are illustrated in figure 4.

The dependence of ϕ_A , ϕ_B and $\frac{\Delta l_A}{l}$, $\frac{\Delta l_B}{l}$ on the commencement scale of inflation is shown in table 1. We see that the fraction of initial conditions that leads to inadequate inflation, $2\frac{\Delta l_A}{l}$, decreases with an increase in the initial energy scale H_i . This result is also illustrated in figures 13(a) and 13(b) where we compare chaotic inflation with monodromy inflation.

3.2 Monodromy Inflation

A straightforward extension of chaotic inflation, called Axion Monodromy, was discussed in [20, 21] and tested against the CMB in [16]. This model is based on the potential

$$V(\phi) = V_0 \left| \frac{\phi}{m_p} \right|^p \quad (3.2)$$

where $0 < p \leq 1$. In this paper our focus will be on two values of p , namely $p = 1, \frac{2}{3}$. (However our methods are very general and easily carry over to other values of p .)

One should note that for $p \leq 1$ the potential (3.2) is not differentiable at the origin. This might lead to problems with reheating since the latter usually occurs during rapid oscillations

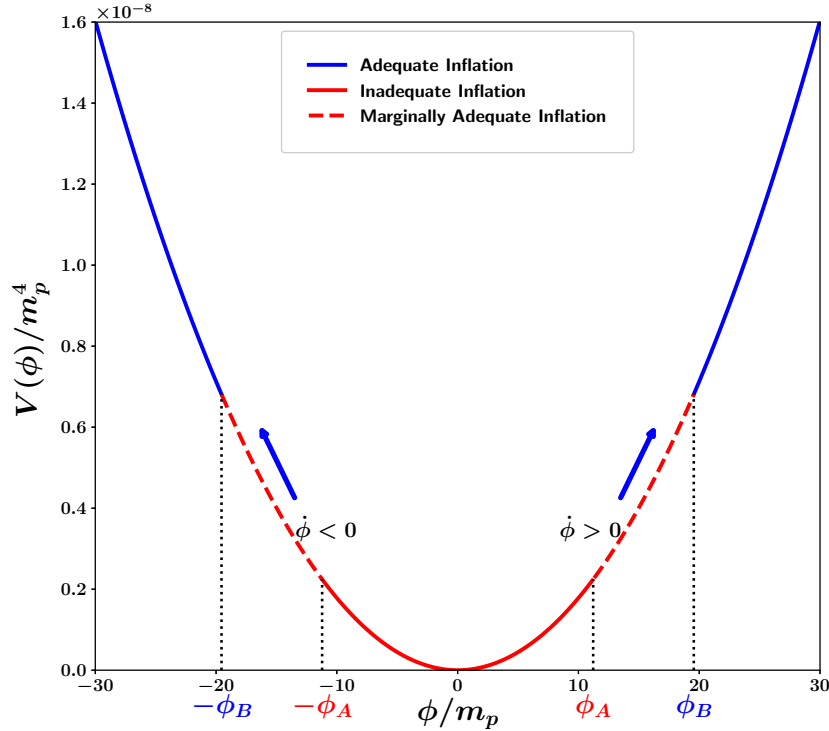


Figure 3: Initial field values, ϕ_i , which lead to adequate inflation with $N_e \geq 60$ (blue), marginally adequate (dashed red) and inadequate (red) inflation are schematically shown for chaotic inflation (3.1). The blue lines represent regions of adequate inflation. Initial values of ϕ_i lying in the blue region result in adequate inflation *irrespective* of the sign of $\dot{\phi}_i$. The red lines come in two styles: dashed/solid and correspond to the following two possibilities: (i) The solid red line represents initial values of ϕ_i for which inflation is never adequate irrespective of the direction of $\dot{\phi}_i$. (ii) In the region shown by the dashed red line one gets adequate inflation only when $\dot{\phi}_i$ is directed towards increasing values of $V(\phi)$ (shown by blue arrows). Note that only a small portion of the full potential is shown in this figure which corresponds to the initial energy scale $H_i = 3 \times 10^{-3} m_p$.

of ϕ around $\phi = 0$. We circumvent this problem by the following useful generalization of (3.2)

$$V(\phi) = V_1 \left| \frac{\phi}{\phi_0} \right|^p \frac{1}{\left[1 + \left(\frac{\phi_0}{\phi} \right)^n \right]^{\frac{2-p}{n}}}, \quad (3.3)$$

where $n > 1$ is an integer (we have taken $n=4$). In this expression the value of ϕ_0 is chosen so that $V(\phi) \sim |\phi|^p$ for $|\phi| \gg |\phi_0|$ whereas $V(\phi) \sim \phi^2$ for $|\phi| \ll |\phi_0|$. It is well known that inflation ends when the slow-roll parameter ϵ in (2.18) grows to unity. Substituting (3.2) in (2.18) and setting $\epsilon \simeq 1$ one finds $\phi_{end} = \frac{p}{\sqrt{2}} m_p$ which can be used to set a value to ϕ_0 , namely $\phi_0 = \phi_{end}$. With this value of ϕ_0 we proceed with a generality analysis for $p = 1$

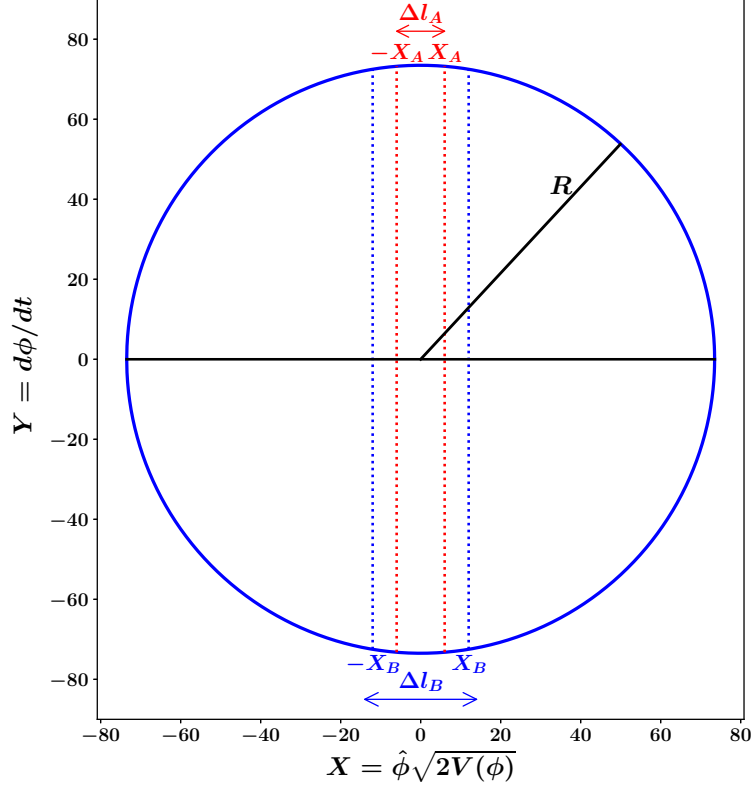


Figure 4: This figure illustrates how one can determine the degree of adequate/inadequate inflation for power law potentials characterizing chaotic inflation and monodromy inflation. The fraction of initial conditions (corresponding to ϕ_A and ϕ_B in figure 3) that leads either to inadequate inflation or marginally adequate inflation, is given by $2\frac{\Delta l_A}{l}$ and $2\frac{\Delta l_B}{l}$ respectively, where $l = 2\pi R$. Adequate inflation with $N_e \geq 60$ is described by the fraction $1 - 2\frac{\Delta l_B}{l}$. ($\hat{\phi} = \frac{\phi}{|\phi|}$ is the sign of field ϕ .)

which will be followed by a similar analysis for $p = 2/3$. (Note that our main results are quite insensitive to the value of ϕ_0 .)

Linear Monodromy Inflation

Consider first the linear potential

$$V(\phi) = V_0 \left| \frac{\phi}{m_p} \right| \quad (3.4)$$

where $V_0 \simeq 1.97 \times 10^{-10} m_p^4$ is in agreement with the CMB [16] (see Appendix A). This potential and its modification via (3.3) is shown in figure 5. We see that for $|\phi| \ll \frac{m_p}{\sqrt{2}}$, the modified potential behaves like ϕ^2 , and rapidly converges to $V \propto |\phi|$ for $|\phi| \gg \frac{m_p}{\sqrt{2}}$.

H_i (in m_p)	ϕ_A (in m_p)	ϕ_B (in m_p)	$2\frac{\Delta l_A}{l}$	$2\frac{\Delta l_B}{l}$
3×10^{-3}	11.22	19.55	5.80×10^{-3}	1.01×10^{-2}
3×10^{-2}	9.33	21.38	4.83×10^{-4}	1.11×10^{-3}
3×10^{-1}	7.47	23.27	3.86×10^{-5}	1.20×10^{-4}

Table 1: Dependence of ϕ_A , ϕ_B , $\frac{\Delta l_A}{l}$ and $\frac{\Delta l_B}{l}$ on the initial energy scale H_i for quadratic chaotic inflation; see figure 4. Here $l = 2\pi R \equiv 2\pi\sqrt{6}H_i/m_p$. Note that the fraction of initial conditions which leads to inadequate inflation, $2\frac{\Delta l_A}{l}$, *decreases* as H_i is increased. The same is true for the fraction of initial conditions giving rise to marginally adequate inflation, $2\frac{\Delta l_B}{l}$. The fraction of initial conditions leading to adequate inflation, with $N_e \geq 60$, is given by $1 - 2\frac{\Delta l_B}{l}$. Thus inflation proves to be more general for larger values of the initial energy scale H_i , since a larger initial region in phase space gives rise to adequate inflation with $N_e \geq 60$.

The phase-space diagram for this potential, shown in figure 6, was obtained by solving the equations (2.15), (2.16), (2.19), (3.4) numerically, for the initial energy scale $H_i = 3 \times 10^{-3}m_p$.

Initial values of ϕ that lead to adequate or inadequate inflation are schematically shown in figure 8. Inadequate inflation arises when the scalar field originates in the region $\phi_i \in [-\phi_A, \phi_A]$, shown by solid red line. Blue lines represent initial field values $\phi_i \in (-\phi_m, -\phi_B) \cup (\phi_B, \phi_m)$, which always result in adequate inflation. Note that ϕ_m is the maximum allowed value of ϕ_i for a given initial energy scale, as determined from the consistency equations (2.14), (2.20). Initial conditions $\phi_i \in [-\phi_B, -\phi_A] \cup [\phi_A, \phi_B]$, shown by dashed red lines, lead to adequate inflation only when ϕ_i points in the direction (shown by blue arrows) of increasing $V(\phi)$. The dependence of ϕ_A and ϕ_B on the initial energy scale H_i is shown in table 2.

The values of $2\frac{\Delta l_A}{l}$ and $2\frac{\Delta l_B}{l}$ in table 2 have been determined by assuming a uniform distribution of initial values of $Y = \dot{\phi}$ and $X = \hat{\phi}\sqrt{2V(\phi)}$ on the circular boundary (2.20). We find that $2\frac{\Delta l_A}{l}$ and $2\frac{\Delta l_B}{l}$ decrease with an increase in H_i , as expected.

Fractional Monodromy Inflation

Next we consider

$$V(\phi) = V_0 \left| \frac{\phi}{m_p} \right|^{\frac{2}{3}} \quad (3.5)$$

where CMB constraints imply $V_0 = 3.34 \times 10^{-10}m_p^4$ [16] (see Appendix A). The potential (3.5) and its generalization (3.3) are shown in figure 9. As expected, the cusp at $\phi \simeq 0$ in (3.5) is absent in the modified potential (3.3), which is shown by the green line in figure 9.

The phase-space diagram for this potential, shown in figure 10, was obtained by solving the equations (2.15), (2.16), (2.19) numerically for the initial energy scale $H_i = 3 \times 10^{-3}m_p$.

Initial values of ϕ that lead to adequate or inadequate inflation are schematically shown in figure 12. Inadequate inflation arises when the scalar field originates in the region $\phi_i \in [-\phi_A, \phi_A]$, shown by solid red lines. Blue lines represent initial field values $\phi_i \in (-\phi_m, -\phi_B) \cup (\phi_B, \phi_m)$, which always result in adequate inflation. Note that ϕ_m is the maximum allowed value of ϕ for a given initial energy scale, as determined from the consistency equations (2.14), (2.20). The initial conditions $\phi_i \in [-\phi_B, -\phi_A] \cup [\phi_A, \phi_B]$, shown by dashed red

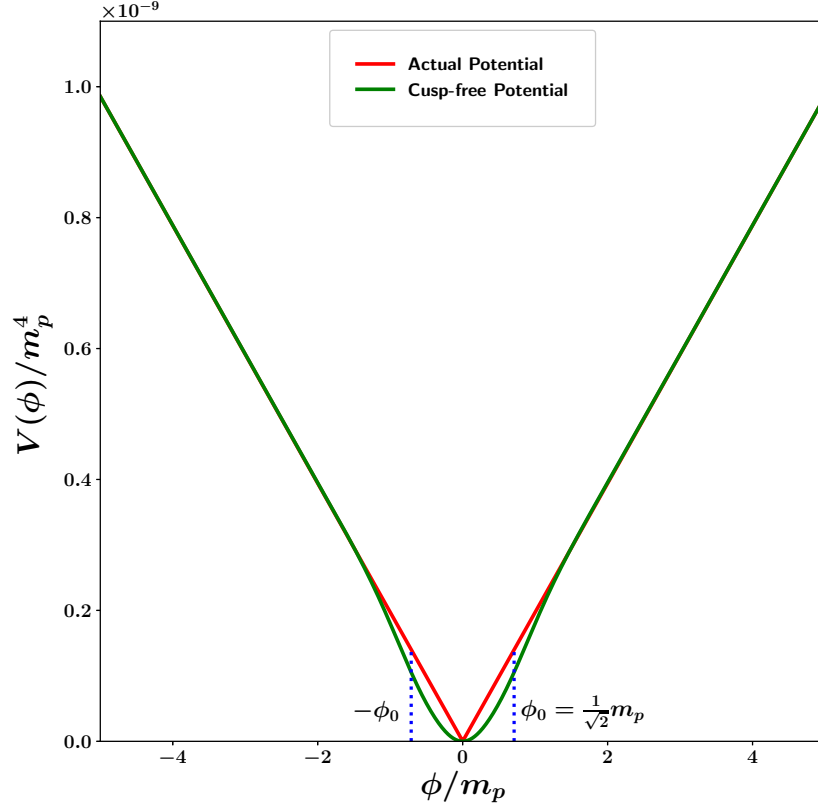


Figure 5: The monodromy potential (3.4) and its cusp-free generalization (3.3) are shown by the red and green curves, respectively. The original potential $V \propto |\phi|$ is not differentiable at the origin which can be problematic when considering oscillations of $\phi(t)$. The modified potential (3.3) corrects this by enabling the potential to behave like $V(\phi) \sim \phi^2$ at the origin. The modified potential rapidly converges to the $V \propto |\phi|$ for $|\phi| \gg m_p/\sqrt{2}$.

lines, lead to adequate inflation only when $\dot{\phi}_i$ points in the direction (shown by blue arrows) of increasing $V(\phi)$. We refer to this as marginally adequate inflation. The dependence of ϕ_A and ϕ_B on the initial energy scale H_i is shown in Table 3.

As in the case of chaotic inflation, we determine the fraction of initial conditions that do not lead to adequate inflation (the degree of inadequate inflation), by assuming a uniform distribution of initial values of $Y = \dot{\phi}$ and $X = \hat{\phi}\sqrt{2V(\phi)}$ on the circular boundary (2.14), (2.20) with $V(\phi)$ given by (3.5). Our results are given in table 3. As was the case for quadratic chaotic inflation, we once more find that $\frac{\Delta l_A}{l}$ and $\frac{\Delta l_B}{l}$ decrease with an increase in H_i ; see table 3, figures 13(a) and 13(b).

3.3 Comparison of power law potentials

In this subsection we compare the generality of inflation for the power law family of potentials, $V \propto |\phi|^p$, by plotting the fraction of initial conditions that *do not lead to* adequate inflation

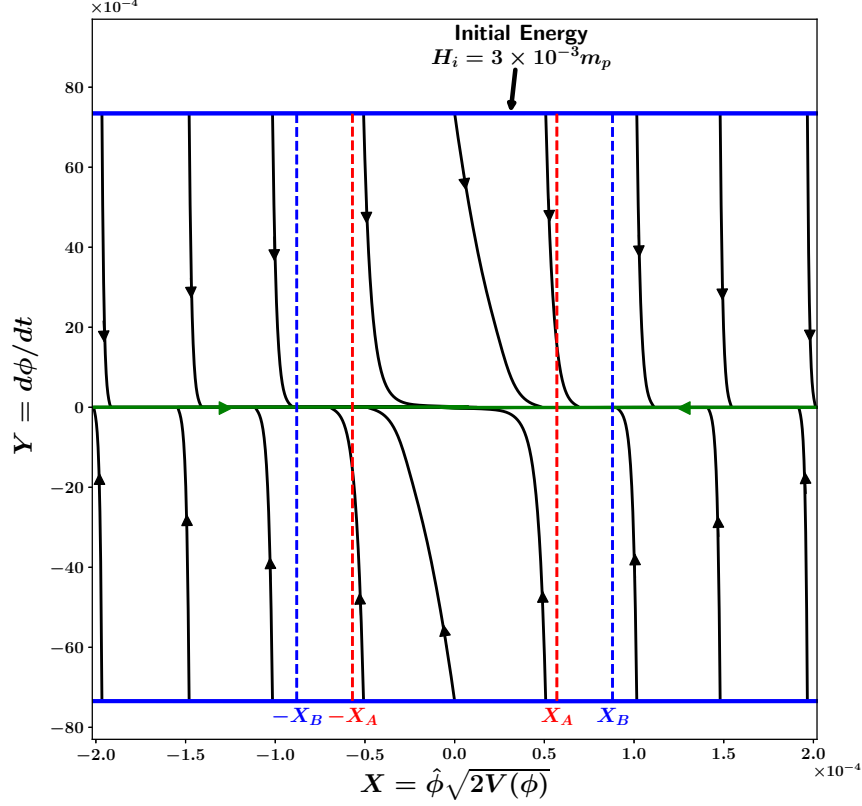


Figure 6: This figure shows a portion of the phase-space of monodromy inflation $V \propto |\phi|$. The variable Y ($= \dot{\phi}$) is plotted against X ($= \hat{\phi}\sqrt{2V(\phi)}$). ($\hat{\phi} = \frac{\phi}{|\phi|}$ is the sign of field ϕ .) The initial conditions are specified on arcs which form the blue colored boundary. Note that these arcs correspond to a *very small portion* of the full ‘initial conditions’ circle R , and therefore appear to be straight lines. In this analysis we assume $R = \sqrt{6}H_i/m_p$, with $H_i = 3 \times 10^{-3}m_p$. We find that, commencing at the boundary, most solutions quickly converge to the two slow-roll inflationary separatrices (green horizontal lines) before travelling to the origin where $\{\dot{\phi}, \phi\} = \{0, 0\}$. A blow up of the central portion of this figure is shown in figure 7.

($2\frac{\Delta l_A}{l}$ and $2\frac{\Delta l_B}{l}$) in figures 13(a) and 13(b); also see tables 1-3. These figures demonstrate that the set of initial conditions which give rise to adequate inflation (with $N_e \geq 60$) increases with the energy scale of inflation, H_i . We also find that inflation is sourced by a larger set of initial conditions for the monodromy potential $V \propto |\phi|^{\frac{2}{3}}$, which is followed by $V \propto |\phi|$ and $V \propto \phi^2$ respectively. Finally we draw attention to the fact that our conclusions remain unchanged if we determine the degree of inflation by a different measure such as $\frac{\Delta\phi_A}{\phi_{max}}$ and $\frac{\Delta\phi_B}{\phi_{max}}$, where ϕ_{max} is the maximum allowed value of ϕ for a given inflationary energy scale.

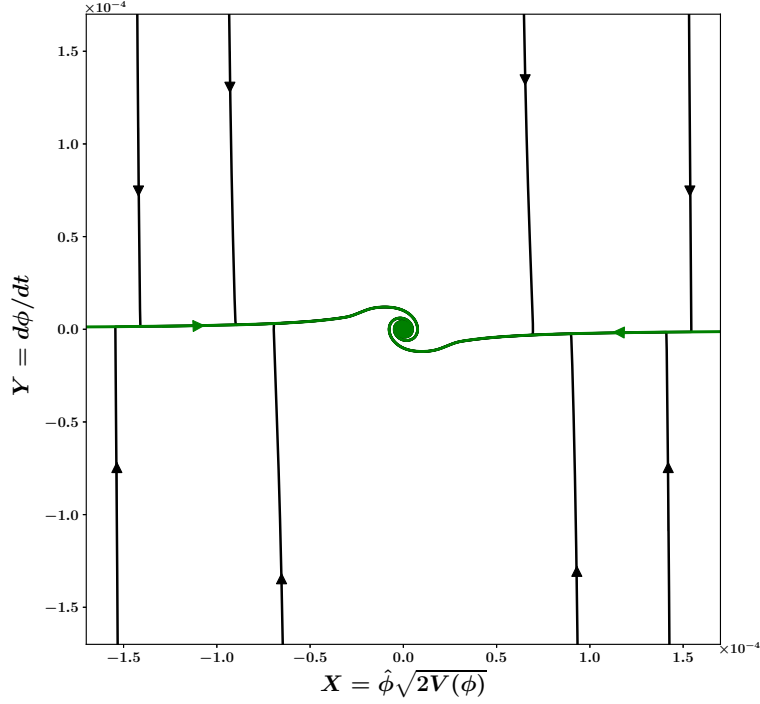


Figure 7: A zoomed-in view of the phase-space of monodromy inflation with $V \propto |\phi|$. Note that scalar field trajectories initially converge towards the slow-roll inflationary separatrices (horizontal green lines), moving from there towards $\phi = 0$, where the field oscillates.

H_i (in m_p)	ϕ_A (in m_p)	ϕ_B (in m_p)	$2\frac{\Delta l_A}{l}$	$2\frac{\Delta l_B}{l}$
3×10^{-3}	6.45	15.29	4.37×10^{-3}	6.73×10^{-3}
3×10^{-2}	4.58	17.18	3.68×10^{-4}	7.13×10^{-4}
3×10^{-1}	2.69	19.06	2.84×10^{-5}	7.51×10^{-5}

Table 2: Dependence of ϕ_A , ϕ_B , $\frac{\Delta l_A}{l}$ and $\frac{\Delta l_B}{l}$ on the initial energy scale H_i for monodromy inflation $V \propto |\phi|$. Here $l = 2\pi R \equiv 2\pi\sqrt{6}H_i/m_p$ and $\frac{\Delta l_A}{l}$, $\frac{\Delta l_B}{l}$ were defined in figure 4. Note that the fraction of initial conditions which leads to inadequate inflation, $2\frac{\Delta l_A}{l}$, decreases as H_i is increased. The same is true for the fraction of initial conditions giving rise to marginally adequate inflation, $2\frac{\Delta l_B}{l}$. The fraction of initial conditions leading to adequate inflation, with $N_e \geq 60$, is given by $1 - 2\frac{\Delta l_B}{l}$. Thus inflation proves to be more general for larger values of the initial energy scale H_i , since a larger initial region in phase space gives rise to adequate inflation with $N_e \geq 60$.

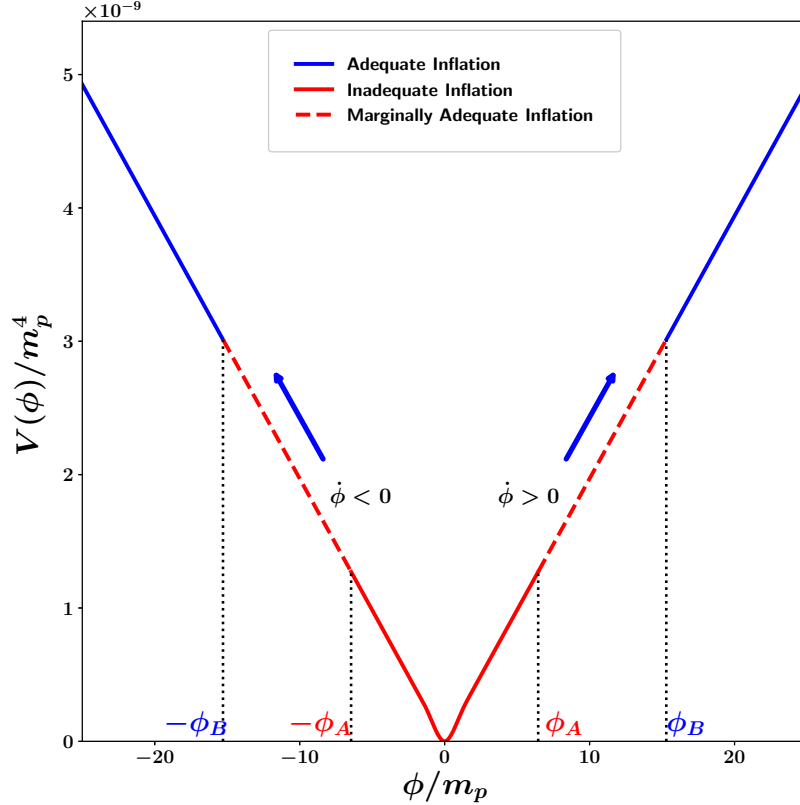


Figure 8: This figure schematically shows initial field values which result in adequate inflation with $N_e \geq 60$ (blue), marginally adequate (dashed red) and inadequate inflation (red) for the monodromy potential $V \propto |\phi|$ modified by (3.3) with $p = 1$ and $\phi_0 = \frac{m_p}{\sqrt{2}}$. The initial energy scale is $H_i = 3 \times 10^{-3} m_p$. As earlier, blue lines represent regions of adequate inflation. The red lines come in two styles: dashed/solid and correspond to the two possible initial directions of $\dot{\phi}$. The solid red line represents initial values of ϕ for which inflation is never adequate irrespective of the direction of $\dot{\phi}_i$. In the region shown by the dashed line one gets adequate inflation only when $\dot{\phi}_i$ points in the direction (shown by blue arrows) of increasing $V(\phi)$. Note that only a small portion of the full potential is shown in this figure.

4 Higgs Inflation

It would undoubtedly be interesting if inflation could be realized within the context of the Standard Model (*SM*) of particle physics. Since the *SM* has only a single scalar degree of freedom, namely the Higgs field, one can ask whether the Higgs field (4.2) can source inflation. Unfortunately the self-interaction coupling of the Higgs field, λ in (4.2), is far too large to be consistent with the small amplitude of scalar fluctuations observed by the cosmic microwave background [16].

This situation can however be remedied if either of the following possibilities is realized:

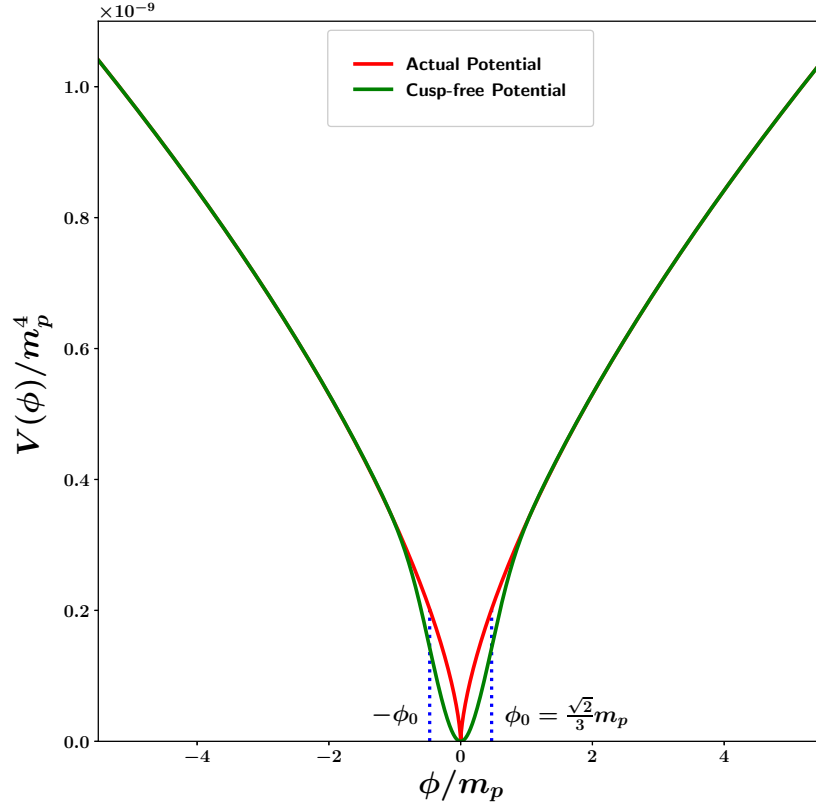


Figure 9: The monodromy potential (3.5) and its cusp-free generalization (3.3) with $p = 2/3$ are shown by the red and green curves, respectively.

(i) the Higgs couples non-minimally to gravity, or (ii) the Higgs field is described by a non-canonical Lagrangian⁴

Indeed, as first demonstrated in [23], inflation can be sourced by the SM Higgs potential if the Higgs field is assumed to couple non-minimally to the Ricci scalar. The resultant inflationary model provides a good fit to observations and has been extensively developed and examined in [23–27]. A different means of sourcing Inflation through the Higgs field was discussed in [14] where it was shown that the SM Higgs potential with a non-canonical kinetic term fits the CMB data very well by accounting for the currently observed values of the scalar spectral index n_s and the tensor-to-scalar ratio r . We shall proceed to study Higgs inflation first in the non-minimal framework in section 4.1 followed by the same in the non-canonical framework in section 4.2.

⁴Another means of reconciling the $\frac{1}{4}\lambda\phi^4$ ($\lambda \sim 0.1$) potential with observations is through a field derivative coupling with the Einstein tensor of the form $G^{\mu\nu}\partial_\mu\partial_\nu\phi/M^2$. This approach has been discussed in [22].

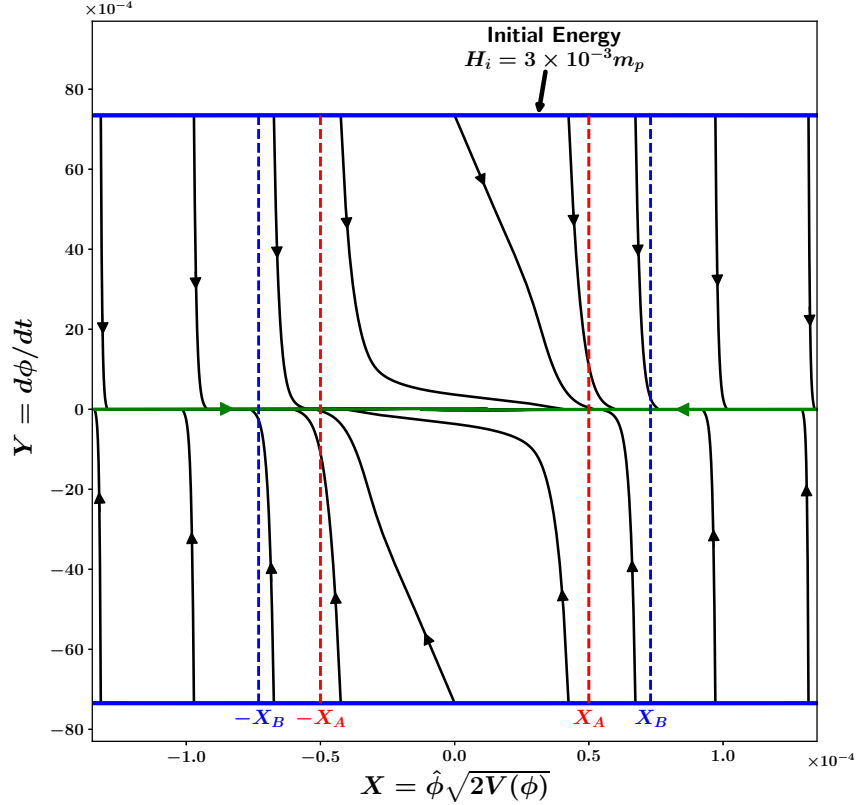


Figure 10: This figure shows a portion of the phase-space of monodromy inflation with $V \propto |\phi|^{2/3}$. The variable Y ($= \dot{\phi}$) is plotted against X ($= \hat{\phi}\sqrt{2V(\phi)}$). ($\hat{\phi} = \frac{\phi}{|\phi|}$ is the sign of field ϕ .) Initial conditions are specified on arcs which form the blue colored boundary. Note that since these arcs correspond to a *very small portion* of the full ‘initial conditions’ circle R , they appear to be straight lines. As in the previous analysis for chaotic inflation we again assume $R = \sqrt{6}H_i/m_p$, with $H_i = 3 \times 10^{-3}m_p$. One finds that, commencing at the boundary, most solutions quickly converge to the two slow-roll inflationary separatrices (green horizontal lines) before travelling to the origin where $\{\dot{\phi}, \phi\} = \{0, 0\}$. A blow up of the central portion of this figure is shown in figure 11.

4.1 Initial conditions for Higgs Inflation in the non-minimal framework

Inflation sourced by the Standard Model (SM) Higgs boson was first discussed in [23]. In this model the Higgs non-minimally couples to gravity with a moderate value of the non-minimal coupling⁵ [24, 25]. The model does not require an additional degree of freedom beyond the SM and fits the observational data quite well [16]. Reheating after inflation in this model has been studied in detail [25, 26] and quantum corrections to the potential at very high

⁵The value of the dimensionless non-minimal coupling $\xi \sim 10^4$ though in itself quite large, is much smaller than the ratio $\left(\frac{m_p}{M_W}\right)^2 \simeq 10^{34}$, where $M_W \sim 100 \text{ GeV}$ is the Electroweak scale.

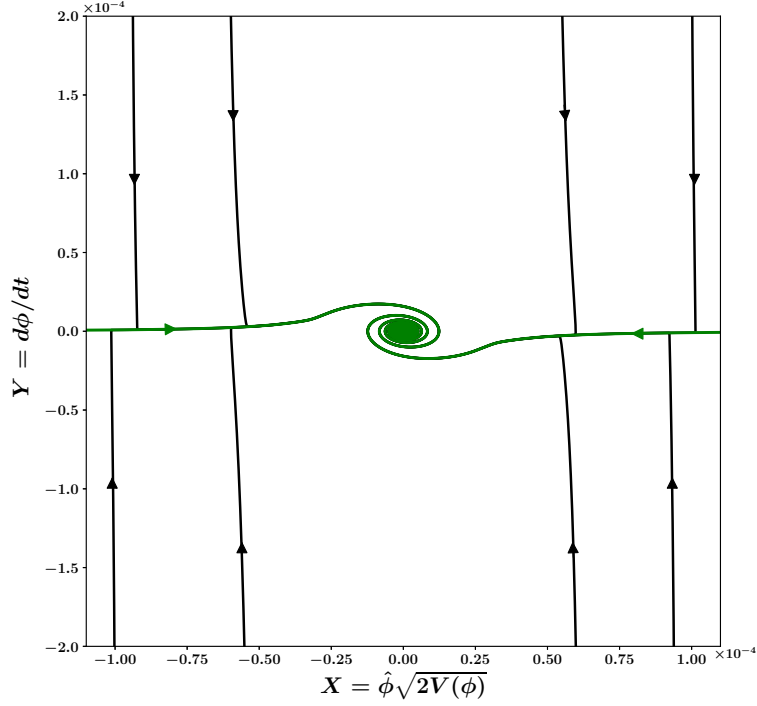


Figure 11: A zoomed-in view of the phase-space of monodromy inflation with $V \propto |\phi|^{2/3}$. One notes that the motion of the scalar field is initially towards the slow-roll inflationary separatrices (horizontal green lines) and from there towards $\phi = 0$, where the field oscillates.

H_i (in m_p)	ϕ_A (in m_p)	ϕ_B (in m_p)	$2 \frac{\Delta l_A}{l}$	$2 \frac{\Delta l_B}{l}$
3×10^{-3}	4.29	13.45	3.64×10^{-3}	5.33×10^{-3}
3×10^{-2}	2.41	15.33	3.0×10^{-4}	5.56×10^{-4}
3×10^{-1}	0.61	17.22	2.08×10^{-5}	5.78×10^{-5}

Table 3: Dependence of ϕ_A , ϕ_B , $\frac{\Delta l_A}{l}$ and $\frac{\Delta l_B}{l}$ on the initial energy scale H_i for monodromy inflation with $p = \frac{2}{3}$. Here $l = 2\pi R \equiv 2\pi\sqrt{6}H_i/m_p$ and $\frac{\Delta l_A}{l}$, $\frac{\Delta l_B}{l}$ were defined in figure 4. Note that the fraction of initial conditions which leads to inadequate inflation, $2\frac{\Delta l_A}{l}$, decreases as H_i is increased. The same is true for the fraction of initial conditions giving rise to marginally adequate inflation, $2\frac{\Delta l_B}{l}$. The fraction of initial conditions leading to adequate inflation, with $N_e \geq 60$, is given by $1 - 2\frac{\Delta l_B}{l}$. Thus inflation proves to be more general for larger values of the initial energy scale H_i , since a larger initial region in phase space gives rise to adequate inflation with $N_e \geq 60$.

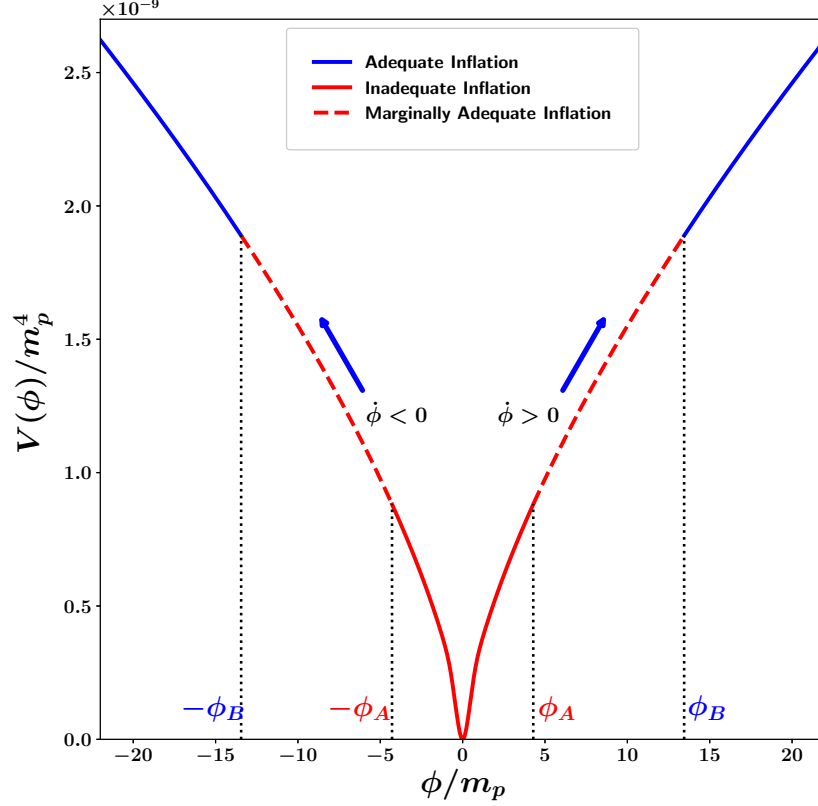


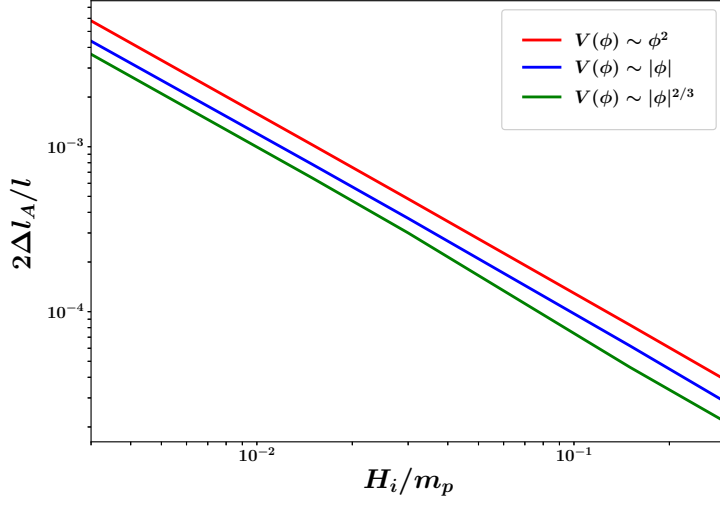
Figure 12: This figure schematically shows initial field values which result in adequate inflation with $N_e \geq 60$ (blue), marginally adequate (dashed red) and inadequate inflation (red) for the monodromy potential (3.5) modified by (3.3). The initial energy scale is $H_i = 3 \times 10^{-3} m_p$. As earlier, blue lines represent regions of adequate inflation. The red lines come in two styles: dashed/solid and correspond to the two possible initial directions of $\dot{\phi}$. The solid red line represents initial values of ϕ for which inflation is never adequate irrespective of the direction of $\dot{\phi}_i$. In the region shown by the dashed red line one gets adequate inflation only when $\dot{\phi}_i$ points in the direction (shown by blue arrows) of increasing $V(\phi)$. Note that only a small portion of the full potential is shown in this figure.

energies have been shown to be small [27]. In this section we assess the generality of Higgs inflation (in the Einstein frame) and determine the range of initial conditions which gives rise to adequate inflation (with $N_e \geq 60$) for a given value of the initial energy scale.

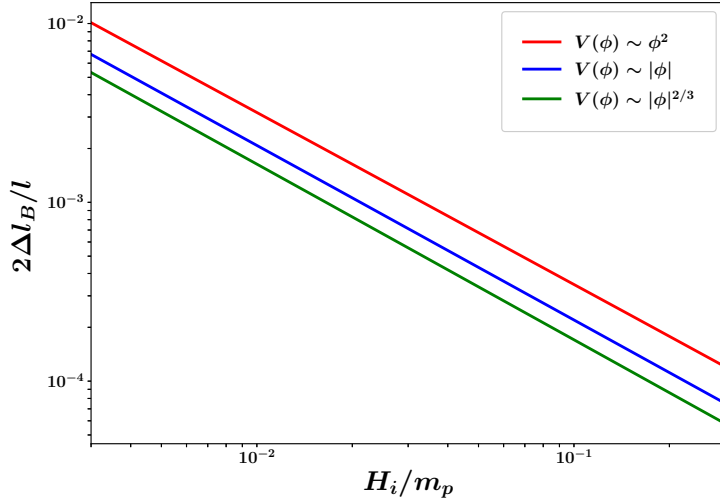
Action for Higgs Inflation

The action for a scalar field ϕ which couples non-minimally to gravity (*i.e.* in the Jordan frame) is given by [23, 24, 28]

$$S_J = \int d^4x \sqrt{-g} \left[f(\phi) R - \frac{1}{2} g^{\mu\nu} \partial_\mu \phi \partial_\nu \phi - U(\phi) \right] \quad (4.1)$$



(a)



(b)

Figure 13: This figure shows the fraction of initial conditions that leads to (a) inadequate inflation, $2\frac{\Delta l_A}{l}$ and (b) marginally adequate inflation, $2\frac{\Delta l_B}{l}$, plotted against the initial energy scale of inflation, H_i . For the definition of $\frac{\Delta l_A}{l}$ and $\frac{\Delta l_B}{l}$, see figure 4. The red curve shows results for $V \propto \phi^2$ while the blue and green curves represent monodromy potentials with $V \propto |\phi|, |\phi|^{2/3}$ respectively. The decrease in $2\frac{\Delta l_A}{l}$ and $2\frac{\Delta l_B}{l}$, which accompanies an increase in H_i is indicative of the fact that the set of initial conditions which give rise to adequate inflation (with $N_e \geq 60$) increases with the energy scale of inflation, H_i . This figure also demonstrates that inflation is sourced by a larger set of initial conditions for the monodromy potential $V \propto |\phi|^{2/3}$, which is followed by $V \propto |\phi|$ and finally $V \propto \phi^2$.

where R is the Ricci scalar and $g_{\mu\nu}$ is the metric in the Jordan frame. The potential for the SM Higgs field is given by

$$U(\phi) = \frac{\lambda}{4}(\phi^2 - \sigma^2)^2 \quad (4.2)$$

where σ is the vacuum expectation value of the Higgs field

$$\sigma = 246 \text{ GeV} = 1.1 \times 10^{-16} m_p \quad (4.3)$$

and the Higgs coupling constant has the value $\lambda = 0.1$. Furthermore

$$f(\phi) = \frac{1}{2}(m^2 + \xi\phi^2) \quad (4.4)$$

where m is a mass parameter given by [28]

$$m^2 = m_p^2 - \xi\sigma^2$$

ξ being the non-minimal coupling constant whose value

$$\xi = 1.62 \times 10^4 \quad (4.5)$$

agrees with observations [16] (see Appendix A). For the above values⁶ of σ and ξ , one finds $m \simeq m_p$, so that

$$f(\phi) \simeq \frac{1}{2}(m_p^2 + \xi\phi^2) = \frac{m_p^2}{2} \left(1 + \frac{\xi\phi^2}{m_p^2}\right). \quad (4.6)$$

We now transfer to the Einstein frame by means of the following conformal transformation of the metric [28]

$$g_{\mu\nu} \longrightarrow \hat{g}_{\mu\nu} = \Omega^2 g_{\mu\nu} \quad (4.7)$$

where the conformal factor is given by

$$\Omega^2 = \frac{2}{m_p^2} f(\phi) = 1 + \frac{\xi\phi^2}{m_p^2}. \quad (4.8)$$

After the field redefinition $\phi \longrightarrow \chi$ the action in the *Einstein frame* is given by [28]

$$S_E = \int d^4x \sqrt{-\hat{g}} \left[\frac{m_p^2}{2} \hat{R} - \frac{1}{2} \hat{g}^{\mu\nu} \partial_\mu \chi \partial_\nu \chi - V(\chi) \right] \quad (4.9)$$

where

$$V(\chi) = \frac{U[\phi(\chi)]}{\Omega^4} \quad (4.10)$$

and

$$\frac{\partial \chi}{\partial \phi} = \pm \frac{1}{\Omega^2} \sqrt{\Omega^2 + \frac{6\xi^2\phi^2}{m_p^2}}. \quad (4.11)$$

Eq. (4.9) describes General Relativity (GR) in the presence of a minimally coupled scalar field χ with the potential $V(\chi)$. (The full derivation of the action in the Einstein frame is given in appendix B.)

⁶Note that the observed vacuum expectation value of the Higgs field $\sigma = 1.1 \times 10^{-16} m_p$ is much smaller than the energy scale of inflation and hence we neglect it in our subsequent calculations.

Limiting cases of the potential in the Einstein Frame

From equations (4.8) and (4.11) one finds the following asymptotic forms for the potential (4.10) (for details see appendix C and [23, 25])

1. For $\phi \ll \sqrt{\frac{2}{3}} \frac{m_p}{\xi}$ one finds

$$\chi = \pm\phi, \quad V(\chi) \simeq \frac{\lambda}{4} \chi^4, \quad |\chi| \ll \sqrt{\frac{2}{3}} \frac{m_p}{\xi}. \quad (4.12)$$

2. For $\sqrt{\frac{2}{3}} \frac{m_p}{\xi} \ll \phi \ll \frac{m_p}{\sqrt{\xi}}$,

$$\chi = \pm \sqrt{\frac{3}{2}} \frac{\xi \phi^2}{m_p}, \quad V(\chi) \simeq \left(\frac{\lambda m_p^2}{6 \xi^2} \right) \chi^2, \quad \sqrt{\frac{2}{3}} \frac{m_p}{\xi} \ll |\chi| \ll \sqrt{\frac{3}{2}} m_p. \quad (4.13)$$

3. For $\phi \gg \frac{m_p}{\sqrt{\xi}}$

$$\chi = \pm \sqrt{6} m_p \log \left(\frac{\sqrt{\xi} \phi}{m_p} \right), \quad V(\chi) \simeq \frac{\frac{\lambda m_p^4}{4 \xi^2}}{\left(1 + \exp \left[-\sqrt{\frac{2}{3}} \frac{|\chi|}{m_p} \right] \right)^2}, \quad |\chi| \gg \sqrt{\frac{3}{2}} m_p \quad (4.14)$$

A good analytical approximation to the potential which can accommodate both (4.13) and (4.14) is

$$V(\chi) \simeq V_0 \left(1 - \exp \left[-\sqrt{\frac{2}{3}} \frac{|\chi|}{m_p} \right] \right)^2, \quad |\chi| \gg \sqrt{\frac{2}{3}} \frac{m_p}{\xi} \quad (4.15)$$

where V_0 is given by (Appendix A)

$$V_0 = \frac{\lambda m_p^4}{4 \xi^2} = 9.6 \times 10^{-11} m_p^4. \quad (4.16)$$

Generality Analysis of Higgs inflation in the Einstein Frame

As we have seen, Higgs inflation in the Einstein frame can be described by a minimally coupled canonical scalar field χ with a suitable potential $V(\chi)$. We have analysed two different limits of the potential $V(\chi)$ which is asymptotically flat and has plateau like arms for $|\chi| \gg 1$. One notes that when $|\chi| \rightarrow 0$, $V(\chi)$ has a tiny kink with amplitude $\frac{\lambda}{4} \sigma^4 \sim 10^{-66} m_p^4$. This kink is much smaller than the maximum height of the potential and can be neglected for all practical purposes. (This is simply a reflection of the fact that the inflation energy scale is much larger than the electro-weak scale.) We have numerically evaluated the potential defined in (4.10) & (4.11) and compared it with the approximate form given in equation (4.15); see figure 14. The difference between the two potentials is shown in figure 15. One finds that the maximum fractional difference between the two potentials is only 0.16% which justifies the use of (4.15) for further analysis.

During Higgs inflation, the slow-roll parameter is given by

$$\epsilon = \frac{m_p^2}{2} \left(\frac{1}{V} \frac{dV}{d\chi} \right)^2 = \frac{4}{3} \frac{1}{\left(\exp \left(\sqrt{\frac{2}{3}} \frac{|\chi|}{m_p} \right) - 1 \right)^2}, \quad (4.17)$$

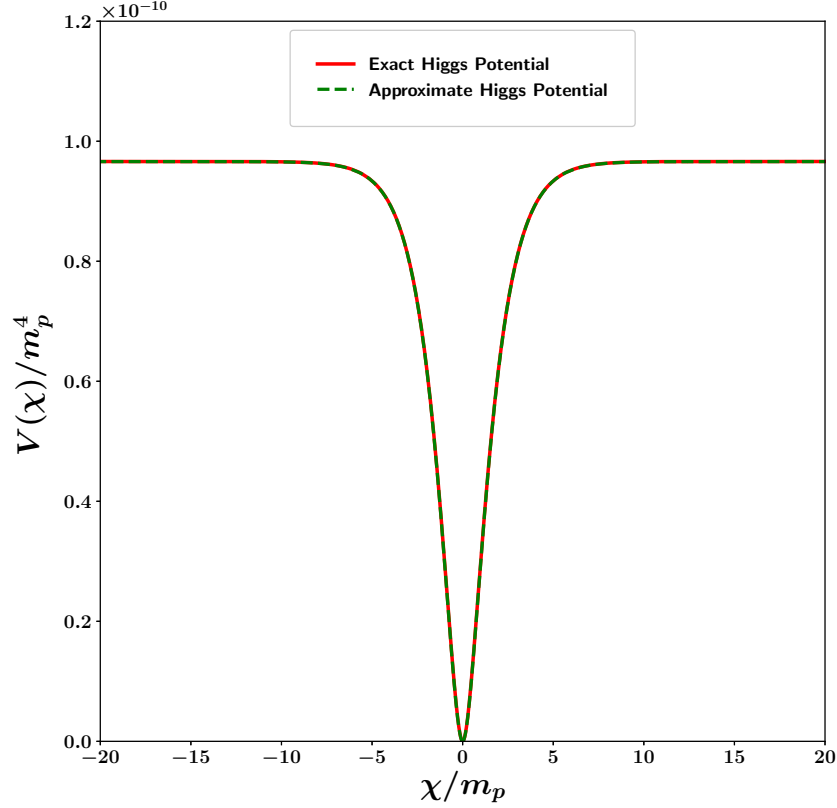


Figure 14: This figure shows the potential for Higgs inflation (in the Einstein frame) in units of m_p^4 . The (solid) red curve shows the numerically determined value of the potential from (4.10) & (4.11), while the (dashed) green curve shows the approximate potential $V(\chi) = V_0 \left(1 - \exp\left[-\sqrt{\frac{2}{3}} \frac{|\chi|}{m_p}\right]\right)^2$. Clearly the approximate form matches the exact one very well.

since slow-roll ends when $\epsilon \simeq 1$, one finds

$$|\chi| \simeq 0.94 \, m_p \sim m_p \, .$$

We study the generality of Higgs inflation in the Einstein frame by plotting the phase-space diagram for the potential (4.15) and determining the region of initial conditions which lead to adequate inflation (*i.e.* $N_e \geq 60$). Our results are shown in figure 16 and a zoomed-in view is presented in figure 17.

We see that the phase-space diagram for Higgs inflation has very interesting properties. The asymptotically flat arms result in robust inflation as expected. However it is also possible to obtain adequate inflation if the inflaton commences from $\chi \simeq 0$. This is because the scalar field is able to climb up the flat wings of $V(\chi)$. This property is illustrated in figure 16 by lines originating in the central region, which are slanted and hence can converge to the slow-roll inflationary separatrices resulting in adequate inflation. This feature is not shared

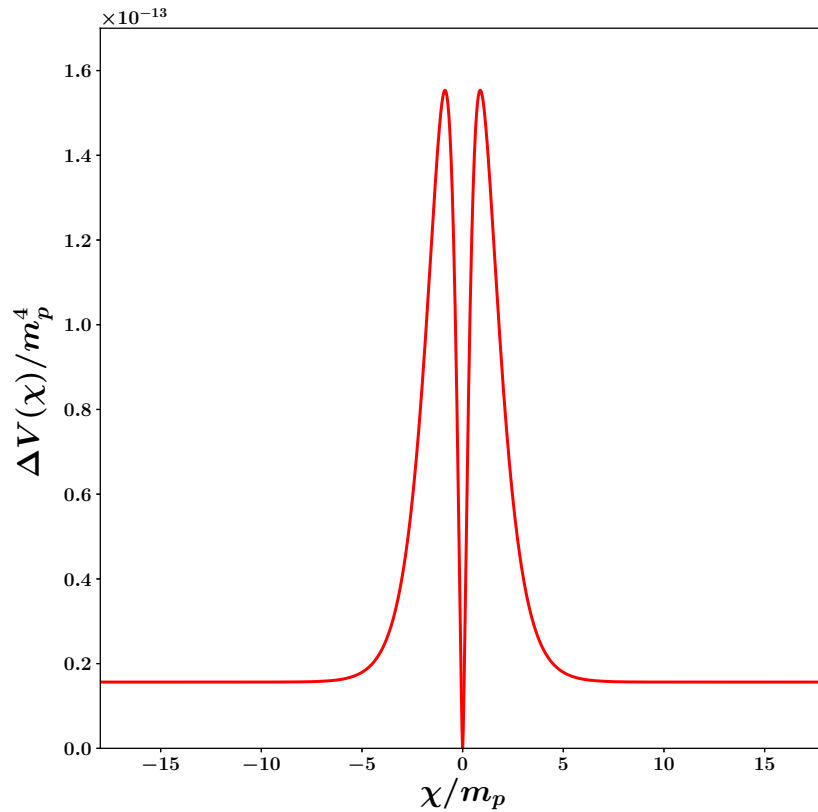


Figure 15: This figure shows the absolute value of the difference between the numerically determined Higgs potential (4.10) & (4.11), and the approximate form (4.15). We see that the maximum difference is near $\chi \sim m_p$ and its fractional value is only 0.16%.

by chaotic inflation where one cannot obtain adequate inflation by starting from the origin (provided the initial energy scale is not too large, *i.e.* $H_i < m_p$.)

This does not however imply that all possible initial conditions lead to adequate inflation in the Higgs scenario. As shown in figure 18 there is a small region of initial field values denoted by $|\chi_A| < |\chi_i| < |\chi_B|$ which does not lead to adequate inflation if χ_i and $\dot{\chi}_i$ have opposite signs (dashed red lines). By contrast, the solid blue lines in the same figure show the region of χ_i that results in adequate inflation *independently of the direction* of the initial velocity $\dot{\chi}_i$. The dependence of χ_A and χ_B on the initial energy scale is shown in table 4 (also see figure 18). Note the surprising fact that the value of $\chi_B - \chi_A$ remains *virtually unchanged* as H_i increases.

The results of figures 16, 17 and 18 lead us to conclude that there is a region lying close to the origin of $V(\chi)$, namely $\chi_i \in (-\chi_A, \chi_A)$, where one gets adequate inflation regardless of the direction of $\dot{\chi}_i$. One might note that this feature is absent in the power law family of potentials described in the previous section (compare figure 18 with figures 3, 8, 12). values that lead to partially adequate inflation, $|\chi_i| \in [|\chi_A|, |\chi_B|]$ We therefore conclude that a wide

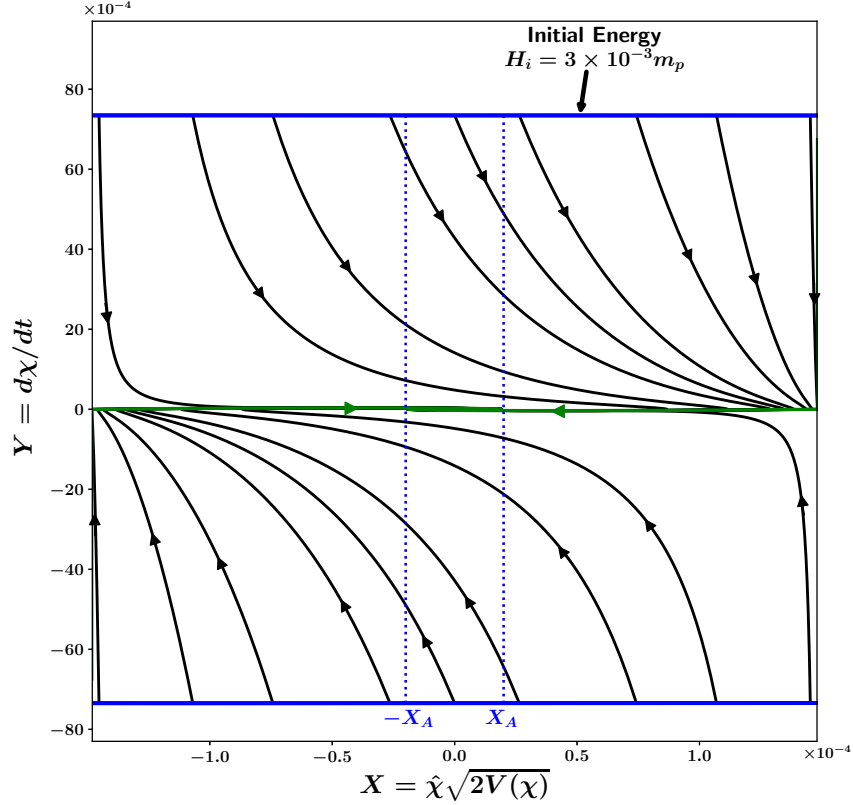


Figure 16: This figure shows the phase-space of Higgs inflation in the Einstein frame. $Y = d\chi/dt$ is plotted against $X = \hat{\chi}\sqrt{2V(\chi)}$ for the initial energy scale $H_i = 3 \times 10^{-3}m_p$. ($\hat{\chi} = \frac{\chi}{|\chi|}$ is the sign of field χ .) We see that commencing from a fixed initial energy (shown by the blue boundary lines), most solutions rapidly converge towards the two inflationary separatrices (horizontal green lines) corresponding to slow-roll inflation. We therefore find that inflation for the Higgs potential is remarkably general and can commence from a very wide class of initial conditions. Note that trajectories lying close to the origin, *i.e.* within the vertical band marked by $(-X_A, X_A)$, are *strongly curved*. This property allows them to converge to the inflationary separatrices giving rise to adequate inflation with $N_e \geq 60$. It is interesting to contrast this behaviour with that of chaotic inflation, shown in figure 1, for which there is a small region with inadequate inflation near the center. Because of this property, the Higgs scenario displays adequate inflation over a slightly larger range of initial conditions when compared with chaotic inflation.

range of initial conditions can generate adequate inflation in the Higgs case, which does not support some of the conclusions drawn in [12].

Finally we would like to draw attention to the fact that the phase-space analysis performed here for Higgs inflation is likely to carry over to the T-model α -attractor potential [29], since the two potentials are qualitatively very similar.

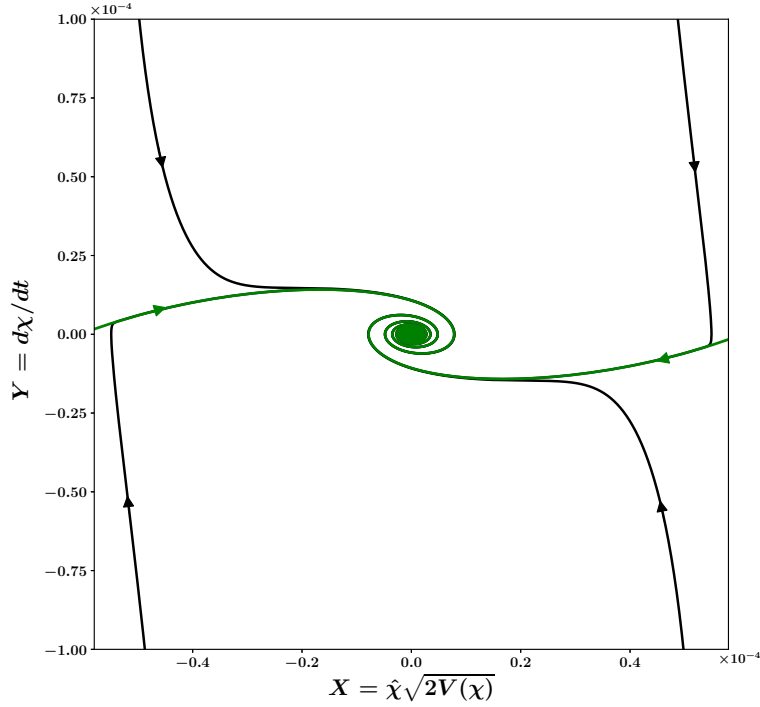


Figure 17: A zoomed-in view of the central region in figure 16. We see that most trajectories (associated with different initial conditions) initially converge towards the horizontal slow-roll inflationary separatrics (green lines) before spiralling in towards the center. (The spiral reflects oscillations of the inflaton about the minimum of its potential.)

H_i (in m_p)	χ_A (in m_p)	χ_B (in m_p)	$\chi_B - \chi_A$ (in m_p)
3×10^{-3}	0.28	11.11	10.83
3×10^{-2}	2.16	12.99	10.83
3×10^{-1}	4.04	14.87	10.83

Table 4: Dependence of χ_A and χ_B on the initial energy scale H_i for Higgs inflation (also see figure 18).

4.2 Initial conditions for Higgs Inflation in the non-canonical framework

The class of initial conditions leading to sufficient inflation widens considerably if we choose to work with scalar fields possessing a non-canonical kinetic term.

The Lagrangian for this class of models is [30]

$$\mathcal{L}(\phi, F) = -F \left(\frac{F}{M^4} \right)^{\alpha-1} - V(\phi), \quad (4.18)$$

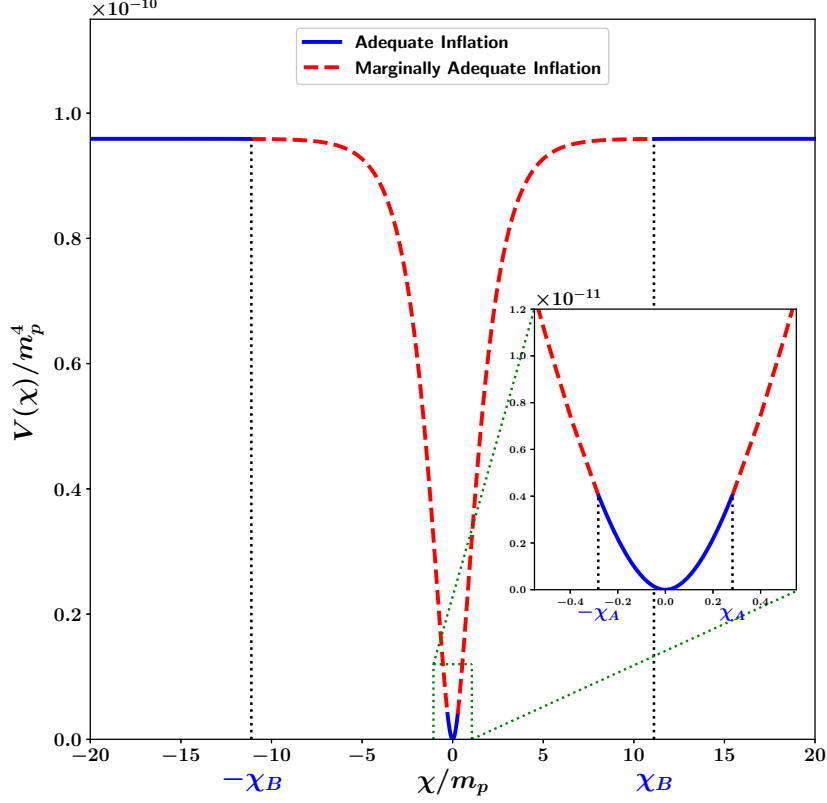


Figure 18: This figure shows initial field values, χ_i , which either lead to adequate inflation (solid blue lines) or partially adequate inflation (dashed red lines). The region corresponding to $\chi_i \in [-\chi_B, -\chi_A] \cup [\chi_A, \chi_B]$ (dashed red) leads to partially adequate inflation. Initial field values originating in this region result in inadequate inflation only when $\dot{\chi}_i$ is directed towards decreasing values of $V(\chi)$. The alternative case, with $\dot{\chi}_i$ directed towards increasing $V(\chi)$, leads to adequate inflation for the same subset $\chi_i \in [-\chi_B, -\chi_A] \cup [\chi_A, \chi_B]$. This figure is shown for an initial energy scale $H_i = 3 \times 10^{-3} m_p$. The precise values of χ_A and χ_B depend on the initial energy scale H_i as shown in table 4. Note that only a small portion of the full potential is shown in this figure.

where $F = \frac{1}{2} \partial_\mu \phi \partial^\mu \phi$, M has the dimensions of mass and α is a dimensionless parameter. The associated energy density and pressure in a FRW universe are given by [14, 30]

$$\rho_\phi = -(2\alpha - 1)F \left(\frac{F}{M^4} \right)^{\alpha-1} + V(\phi), \quad (4.19)$$

$$p_\phi = -F \left(\frac{F}{M^4} \right)^{\alpha-1} - V(\phi), \quad F = -\frac{1}{2} \dot{\phi}^2, \quad (4.20)$$

which reduce to the canonical form $\rho_\phi = -F + V$, $p_\phi = -F - V$ when $\alpha = 1$. The two

Friedmann equations now acquire the form

$$H^2 = \frac{8\pi G}{3} \left[-(2\alpha - 1)F \left(\frac{F}{M^4} \right)^{\alpha-1} + V(\phi) \right], \quad (4.21)$$

$$\frac{\ddot{a}}{a} = -\frac{8\pi G}{3} \left[-(\alpha + 1)F \left(\frac{F}{M^4} \right)^{\alpha-1} - V(\phi) \right], \quad (4.22)$$

and the equation of motion of the scalar field becomes

$$\ddot{\phi} + \frac{3}{2\alpha - 1} H \dot{\phi} + \left(\frac{V'(\phi)}{\alpha(2\alpha - 1)} \right) \left(\frac{2M^4}{\dot{\phi}^2} \right)^{\alpha-1} = 0, \quad (4.23)$$

which reduces to (2.16) when $\alpha = 1$.

Before discussing Higgs inflation in the non-canonical framework, we first examine the inflationary slow-roll parameter ϵ_{nc} which, for non-canonical inflation, is given by [14]

$$\epsilon_{nc} = \left(\frac{1}{\alpha} \right)^{\frac{1}{2\alpha-1}} \left(\frac{3M^4}{V} \right)^{\frac{\alpha-1}{2\alpha-1}} (\epsilon_c)^{\frac{\alpha}{2\alpha-1}}, \quad (4.24)$$

ϵ_c being the canonical slow-roll parameter (2.18). Note that $\epsilon_{nc} < \epsilon_c$ for $3M^4 \ll V$. This suggests that for a fixed potential V , the duration of inflation can be enhanced relative to the canonical case ($\alpha = 1$), by a suitable choice of M .

The Higgs potential

It is well known that the standard model Higgs boson, when coupled minimally to gravity, cannot provide a working model of inflation due to the large value of the coupling constant, $\lambda \simeq 0.1$, in the potential

$$V(\phi) = \frac{\lambda}{4} (\phi^2 - \sigma^2)^2, \quad (4.25)$$

where σ is the vacuum expectation value of the Higgs field (4.3). Indeed $\lambda \simeq 0.1$ is many orders of magnitude larger than the CMB constrained value $\lambda_c \simeq 1.43 \times 10^{-13}$ in the canonical framework (see Appendix A). Additionally the potential (4.25) gives too small a value for the inflationary scalar spectral index n_s and too large a value for the tensor-to-scalar ratio r , to be in accord with observations.

However the situation changes when one examines the potential (4.25) in the non-canonical framework. The expression for the inflationary scalar spectral index now becomes [14]

$$n_s = 1 - \left(\frac{\gamma + 4}{N_e \gamma + 2} \right), \quad (4.26)$$

where

$$\gamma \equiv \frac{2(3\alpha - 2)}{2\alpha - 1}. \quad (4.27)$$

Since γ increases from $\gamma = 2$ for $\alpha = 1$ to $\gamma = 3$ for $\alpha \gg 1$, therefore the scalar spectral index *increases* from the canonical value $n_s = 0.951$ ($\alpha = 1, N_e = 60$) to $n_s = 0.962$, in non-canonical models (with $\alpha \gg 1$).

Similarly one can show that the tensor-to-scalar ratio declines in non-canonical models. For the Higgs potential one gets [14]

$$r = \left(\frac{1}{\sqrt{2\alpha - 1}} \right) \left(\frac{32}{N_e \gamma + 2} \right), \quad (4.28)$$

which demonstrates that the value of r decreases with an increase in the non-canonical parameter α . Figure 19 shows n_s , r plotted as functions of α . One finds that $n_s \simeq 0.96$, $r < 0.1$ for $\alpha \geq 3$, which agrees well with CMB observations.

The relation between the value of the Higgs self-coupling $\lambda \simeq 0.1$ in the non-canonical framework and the corresponding canonical value λ_c is given by [14]

$$\lambda = 4 \left[\frac{32\lambda_c(N_e + 1)^3}{\sqrt{2\alpha - 1}} \left(\frac{\alpha}{4} \left(\frac{1}{6} \frac{m_p^4}{M^4} \right)^{\alpha-1} \right)^{\frac{2}{3\alpha-2}} \left(\frac{1}{N_e \gamma + 2} \right)^{\frac{\gamma+4}{\gamma}} \right]^{\frac{3\alpha-2}{\alpha}}, \quad (4.29)$$

where consistency with CMB observations suggests $\lambda_c \sim 10^{-13}$.

Figure 20 describes the values of the non-canonical parameters α and M that yield $\lambda \simeq 0.1$ in (4.25) – the relation between M and α being provided by equation (4.29). In our subsequent analysis we choose $\alpha = 5$ for simplicity. This is shown by the black color dot in figure 19(a) and 19(b). (The corresponding value of M is shown by the green dot in figure 20.)

As in the case of canonical scalar fields (2.20), one can rewrite the Friedman equation for non-canonical scalars (4.21) as follows

$$R^2 = Y_{nc}^2 + X^2 \quad (4.30)$$

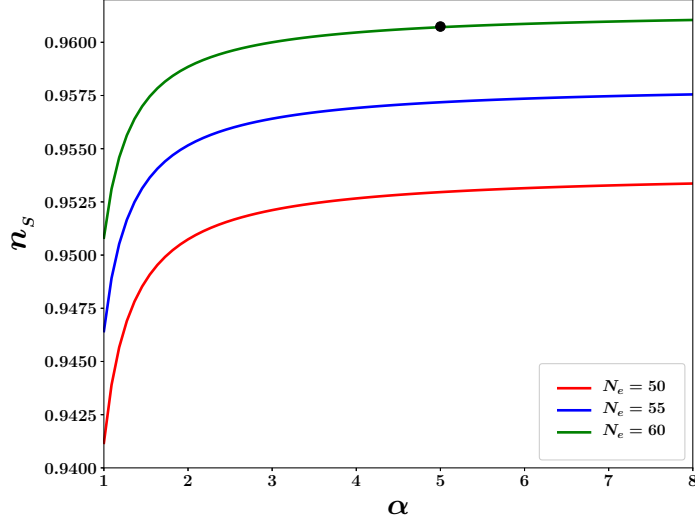
where

$$R = \sqrt{6} \frac{H}{m_p}, \quad X = \hat{\phi} \frac{\sqrt{2V(\phi)}}{m_p^2}, \quad Y_{nc} = \left[2(2\alpha - 1) \left(-\frac{F}{m_p^4} \right) \left(\frac{F}{M^4} \right)^{\alpha-1} \right]^{1/2}. \quad (4.31)$$

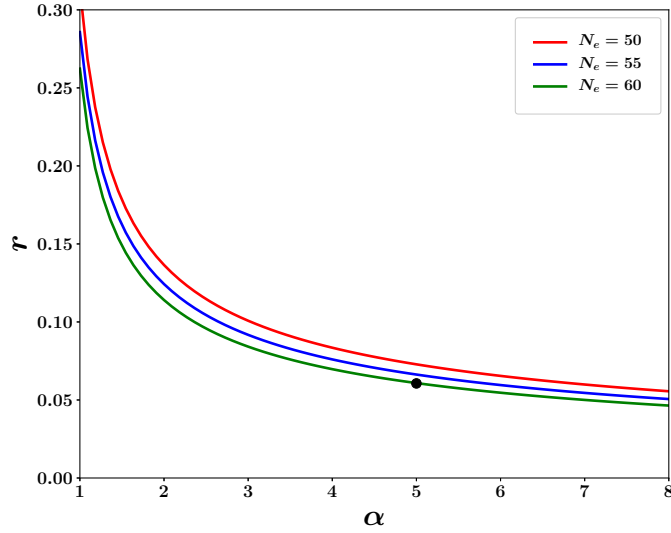
Therefore commencing at some initial value of R ($\equiv \sqrt{6}H/m_p$) one can set different initial conditions by varying X and Y_{nc} . Since X , Y_{nc} satisfy the constraint equation (4.30) they lie on the boundary of a circle.

We probe the robustness of this model to initial conditions by plotting its phase-space diagram (Y_{nc} vs X) and determining the region of initial conditions which gives rise to adequate inflation ($N_e \geq 60$) for values of M and α which satisfy CMB constraints (shown by the green dot in figure 20). The phase-space diagram corresponding to an initial energy scale $H_i = 3 \times 10^{-3} m_p$ is shown in figure 21.

The fraction of initial conditions which give rise to inadequate inflation, $\frac{2\Delta l_A}{l}$, and partially adequate inflation, $\frac{2\Delta l_B}{l}$, are shown in table 5. (As earlier, a uniform distribution of X and Y_{nc} on the boundary of initial conditions has been assumed.) From this table one finds that the values of ϕ_A and ϕ_B associated with an initial energy scale H_i , are much smaller than their counterparts for canonical inflation (see figures 22(a), 22(b) and 23). This is a consequence of the fact that for identical potentials, the slow-roll parameter in the non-canonical case is much smaller than its canonical counterpart ($\epsilon_{nc} \ll \epsilon_c$), which permits inflation to commence from *smaller values* of the inflaton field in the non-canonical case. We also find



(a)



(b)

Figure 19: This figure shows: **(a)** the scalar spectral index n_s , **(b)** the tensor to scalar ratio r , as functions of the non-canonical parameter α and described respectively by equations (4.26) and (4.28). Three values of the number of e-foldings, $N_e = 50, 55$ and 60 , are chosen. One finds that larger values of α result in higher values of n_s and lower values of r . The black dot in both figures indicates the value of α , and the corresponding values of n_s and r , used in our subsequent analysis.

that the fraction of non-inflationary initial conditions, $\frac{\Delta I_A}{I}$, decreases with an increase H_i , as expected.

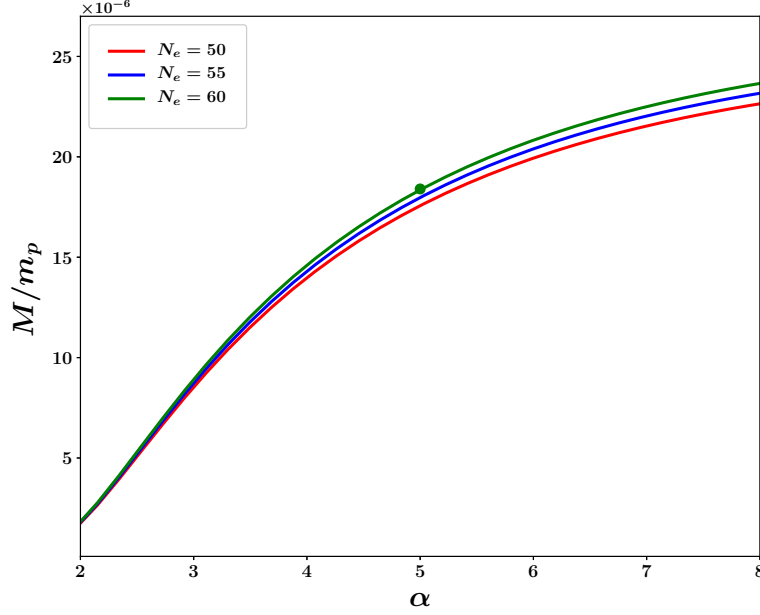


Figure 20: This figure illustrates the relation between the non-canonical parameters M and α , given by equation (4.29), which results in the self-coupling value $\lambda = 0.1$ in equation (4.25). Results for three different e-folding values $N_e = 50, 55, 60$ are shown. The green dot indicates the value of M and α which is used in our subsequent analysis.

H_i (in m_p)	ϕ_A (in m_p)	ϕ_B (in m_p)	$2\frac{\Delta l_A}{l}$	$2\frac{\Delta l_B}{l}$
3×10^{-3}	8.74×10^{-3}	9.07×10^{-3}	1.48×10^{-3}	1.59×10^{-3}
3×10^{-2}	8.66×10^{-3}	8.99×10^{-3}	1.45×10^{-4}	1.57×10^{-4}
3×10^{-1}	8.58×10^{-3}	8.91×10^{-3}	1.43×10^{-5}	1.54×10^{-5}

Table 5: Dependence of ϕ_A , ϕ_B , $\frac{\Delta l_A}{l}$ and $\frac{\Delta l_B}{l}$ on the initial energy scale H_i for non-canonical Higgs inflation. Here $l = 2\pi R \equiv 2\pi\sqrt{6}H_i/m_p$.

In figure 23 we compare values of $\frac{\Delta l_A}{l}$ and $\frac{\Delta l_B}{l}$ for canonical inflation with $V_c(\phi) = \frac{\lambda_c}{4}\phi^4$ and non-canonical inflation⁷ with $V(\phi) = \frac{\lambda}{4}\phi^4$ where λ and λ_c are related by equation (4.29). We find that the values of $\frac{\Delta l_A}{l}$ and $\frac{\Delta l_B}{l}$ are significantly smaller for non-canonical inflation, which implies that inflation arises from a larger class of initial conditions in the non-canonical framework.

⁷Note that the Higgs potential in equation(4.25) can be rewritten as $V(\phi) \simeq \frac{\lambda}{4}\phi^4$, since $\sigma \ll m_p$.

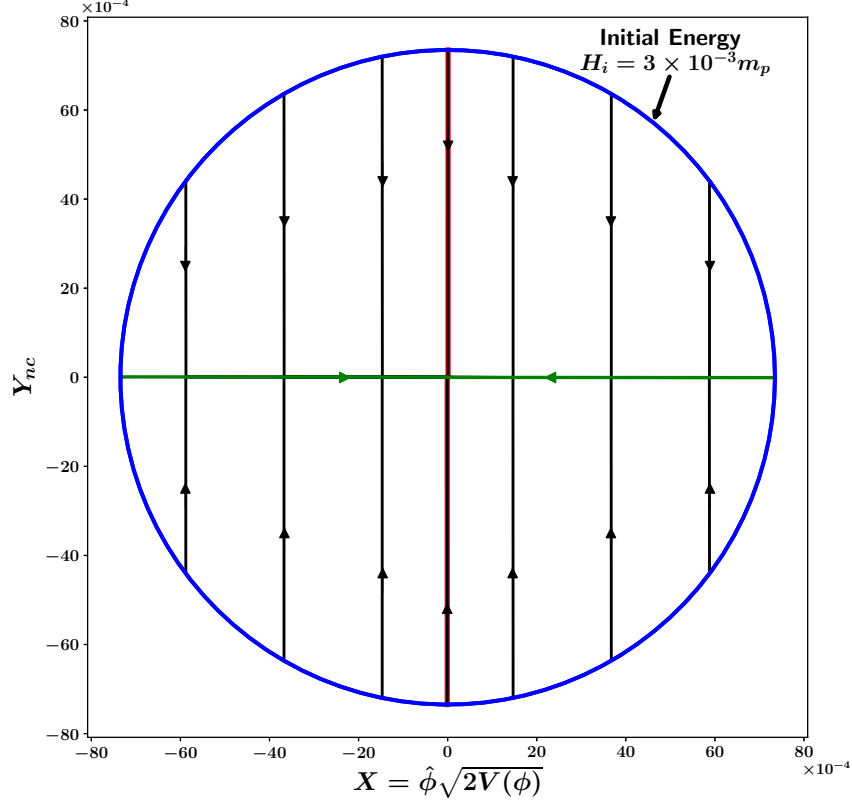


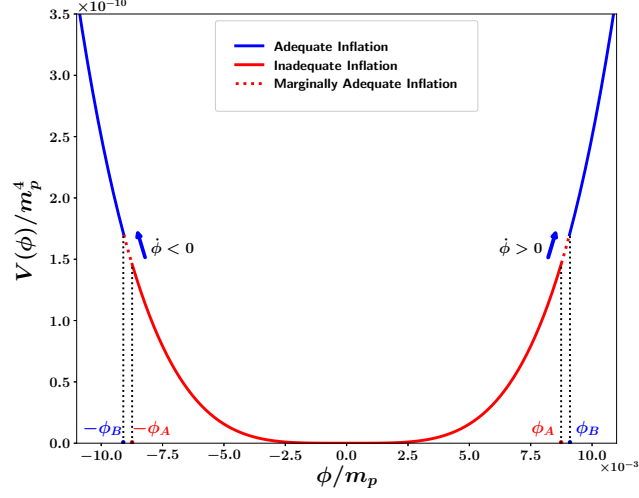
Figure 21: This figure shows the phase-space of Higgs inflation in the non-canonical framework described by (4.25). Y_{nc} , given by (4.31) is plotted against $X (= \hat{\phi} \sqrt{2V(\phi)})$ for different initial conditions all of which commence on the (blue) circle which represents the initial energy scale $H_i = 3 \times 10^{-3} m_p$. ($\hat{\phi} = \frac{\phi}{|\phi|}$ is the sign of field ϕ .) One finds that commencing from the circle, different inflationary trajectories rapidly converge to one of the two inflationary separatrices (green horizontal lines) before proceeding towards the center, which corresponds to the minimum of the potential. The thin vertical central red band corresponds to the region in phase-space that *does not* lead to adequate inflation. Note that this band is *very small* which is indicative of the robustness of Higgs inflation in the non-canonical framework. The arc-length of the red band, when divided by the circumference of the circle with radius $= \sqrt{6} H_i / m_p$, gives the fraction of initial conditions $\frac{2\Delta l_A}{l}$ which lead to inadequate inflation.

5 Starobinsky Inflation

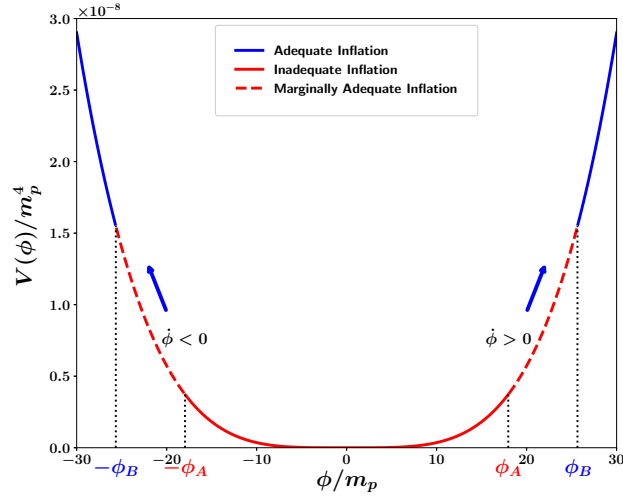
5.1 Action and Potential in the Einstein Frame

Starobinsky inflation [1] is based on the action

$$S = \int d^4x \sqrt{-g} \frac{m_p^2}{2} \left[R + \frac{1}{6m^2} R^2 \right], \quad (5.1)$$

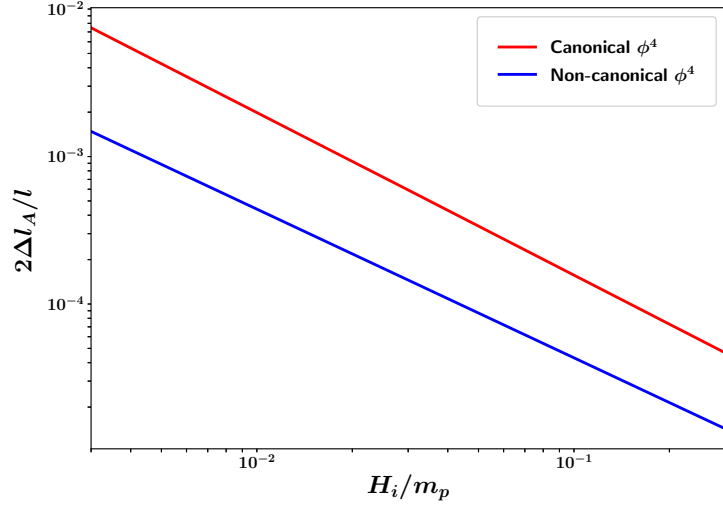


(a)

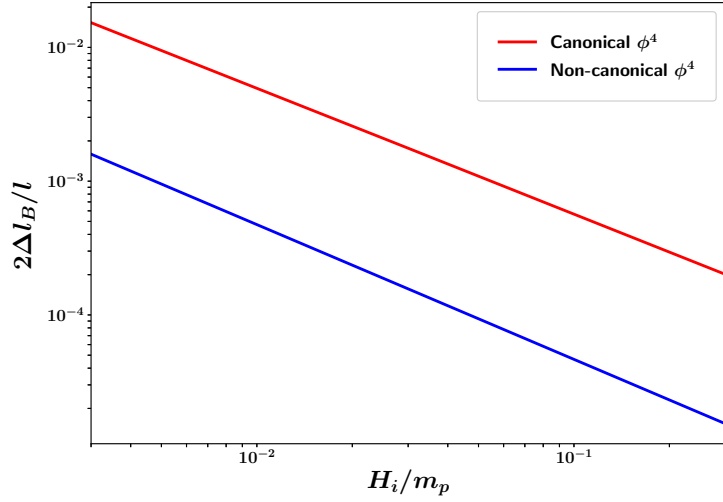


(b)

Figure 22: Initial field values, ϕ_i , which lead to adequate inflation with $N_e \geq 60$ (blue), marginally adequate (dashed red) and inadequate (red) inflation are schematically shown for the Higgs inflation with the quartic potential (4.25): **(a)** in the **non-canonical** framework and **(b)** in the **canonical** framework. The blue lines represent regions of adequate inflation. The red lines come in two styles: dashed/solid and correspond to the two possible initial directions of $\dot{\phi}_i$. The solid red line represents initial values of ϕ for which inflation is never adequate irrespective of the direction of $\dot{\phi}_i$. In the region shown by the dashed line one gets adequate inflation only when $\dot{\phi}_i$ points in the direction of increasing $V(\phi)$. We note that for the non-canonical case, the values of ϕ_A and ϕ_B are extremely small as shown in table 5. (Only a small portion of the full potential is shown in this figure which corresponds to the initial energy scale $H_i = 3 \times 10^{-3} m_p$.)



(a)



(b)

Figure 23: This figure compares the values of (a) $\frac{\Delta l_A}{l}$ and (b) $\frac{\Delta l_B}{l}$ for canonical and non-canonical scalar fields with the potential $V(\phi) \propto \phi^4$. $\frac{\Delta l_A}{l}$ and $\frac{\Delta l_B}{l}$ are shown as functions of the initial energy scale of inflation, H_i . The red and blue curves correspond to canonical and non-canonical quartic inflation respectively. The smaller amplitude of the blue curve in both panels indicates that non-canonical inflation arises for a larger class of initial conditions than canonical inflation (red). The decrease in $\frac{\Delta l_A}{l}$ and $\frac{\Delta l_B}{l}$ with an increase in H_i is indicative of the fact that the set of initial conditions which give rise to adequate inflation (with $N_e \geq 60$) increases with the energy scale of inflation, H_i .

where m is a mass parameter. The corresponding action in the Einstein frame is given by [31, 32]

$$S_E = \int d^4x \sqrt{-g} \left[\frac{m_p^2}{2} \hat{R} - \frac{1}{2} \hat{g}^{\mu\nu} \partial_\mu \phi \partial_\nu \phi - V(\phi) \right] \quad (5.2)$$

where the inflaton potential is

$$V(\phi) = \frac{3}{4}m^2m_p^2\left(1 - e^{-\sqrt{\frac{2}{3}}\frac{\phi}{m_p}}\right)^2 \quad (5.3)$$

and $m = 1.13 \times 10^{-5}m_p$ is required from an analysis of scalar fluctuations [32] (see Appendix A). The potential (5.3) is shown in figure 24.

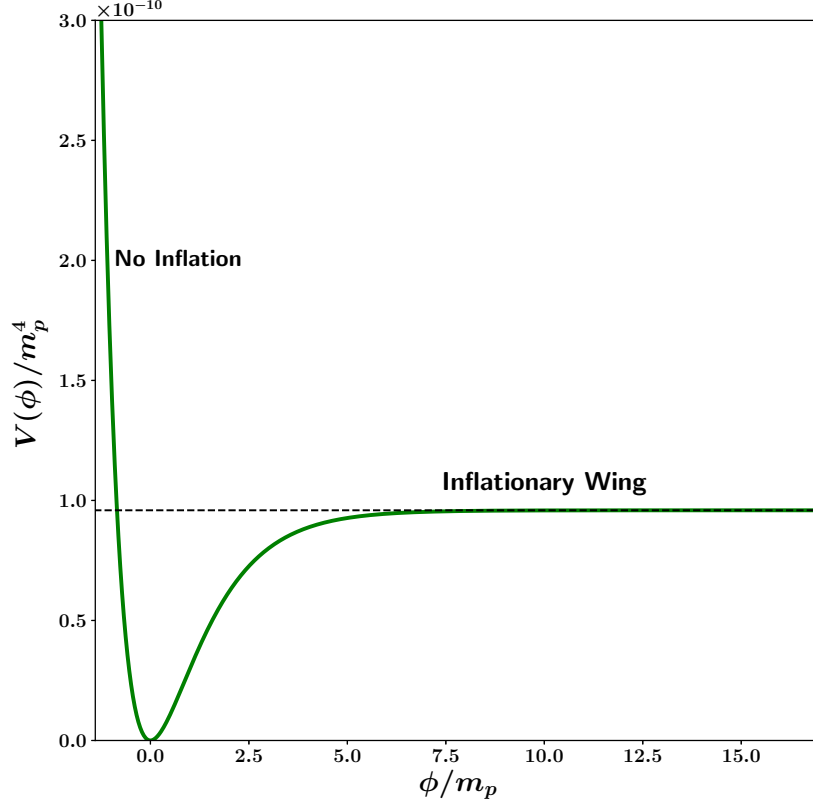


Figure 24: The effective potential in Starobinsky Inflation, (5.3), is plotted in units of m_p^4 . The potential is asymmetric about the origin and has a steep left wing and plateau-like right wing. Inflation occurs along the flat plateau-like right wing, the steep left wing being unable to sustain inflation.

As shown in figure 24, the potential for Starobinsky inflation is asymmetric about the origin. One should note that the flat right wing of the potential has the same functional form as the Higgs inflation potential in the Einstein frame. However the left wing of $V(\phi)$ is very steep. The slow-roll parameter for this potential is given by

$$\epsilon = \frac{4}{3} \left[\exp \left(\sqrt{\frac{2}{3}} \frac{\phi}{m_p} \right) - 1 \right]^{-2}.$$

Inflation occurs for $\epsilon \leq 1$, which corresponds to $\phi \geq 0.94 m_p$ and implies that no inflation can happen on the steep left wing of the potential (for which $\phi < 0$).

5.2 Generality of Starobinsky Inflation

The distinctive properties of the Starobinsky potential discussed above, result in an interesting phase-space, which is shown in figures 26, 27 and 28 for an initial energy scale $H_i = 3 \times 10^{-3} m_p$. A deeper appreciation of this phase-space is obtained by dividing the potential in equation (5.3) into 4 regions A , B , C and D as shown in figure 25. Note that adequate inflation is marked by blue arrows while inadequate inflation is marked by red arrows (this notation has been consistently used throughout our paper). One gets adequate inflation in region D independently of the direction of $\dot{\phi}_i$ (illustrated by blue arrows in region D). Similarly one gets inadequate inflation in region A independently of the direction of $\dot{\phi}_i$ (red arrows). However one gets adequate inflation in region B (called B_+) and C (called C_+) provided $\dot{\phi}_i$ is positive (blue arrows) whereas negative $\dot{\phi}_i$ values in these regions (B_- and C_-) lead to inadequate inflation (red arrows). With this basic picture in mind, we now proceed to discuss the nature of the phase-space in figures 26, 27 and 28.

The asymmetry of the potential (5.3) is reflected in the asymmetry of the phase-space shown in figures 26, 27, 28. The phase-space associated with region A on the steep left wing of $V(\phi)$ shows no slow-roll and consequently does not possess an inflationary separatrix; see figure 26. The flat right wing of $V(\phi)$, on the other hand, has a slow-roll inflationary separatrix ‘S’ (shown by the green line in figures 27 and 28), towards which most trajectories converge; see figures 27, 28. Some of the lines commencing from the left wing with $\dot{\phi} > 0$ initially, represented by B_+ in figure 25, (the brown line in figure 28) are also able to meet the inflationary separatrix giving rise to adequate inflation. These interesting features of Starobinsky inflation have been summarized in figure 25. In this figure, the solid blue line corresponding to $\phi_i \geq \phi_C$ shows trajectories which lead to adequate inflation *regardless of the initial direction of $\dot{\phi}_i$* . By contrast, the red region corresponding to $\phi_i \leq \phi_B$ reflects inadequate inflation. The intermediate region $\phi_i \in [\phi_B, \phi_C]$ leads to adequate inflation only when the initial velocity is positive *i.e.* $\dot{\phi}_i > 0$ (dashed line). Dependence of ϕ_B and ϕ_C on the initial energy scale H_i is shown in table 6.

H_i (in m_p)	ϕ_B (in m_p)	ϕ_C (in m_p)
3×10^{-3}	-0.28	11.11
3×10^{-2}	-2.16	12.99
3×10^{-1}	-4.04	14.87

Table 6: Dependence of ϕ_B and ϕ_C on the initial energy scale H_i for Starobinsky Inflation.

From table 6 one observes that ϕ_B shifts to lower (more negative) values as the initial energy scale of inflation, H_i , is increased. This is indicative of the fact that inflation can commence even from the steep left wing of $V(\phi)$ provided the scalar field has a sufficiently large positive velocity initially, which would enable the inflaton to climb up the flat right wing and result in inflation. ⁸

⁸Pre-inflationary initial conditions for Starobinsky inflation have also been studied in [33] in the context

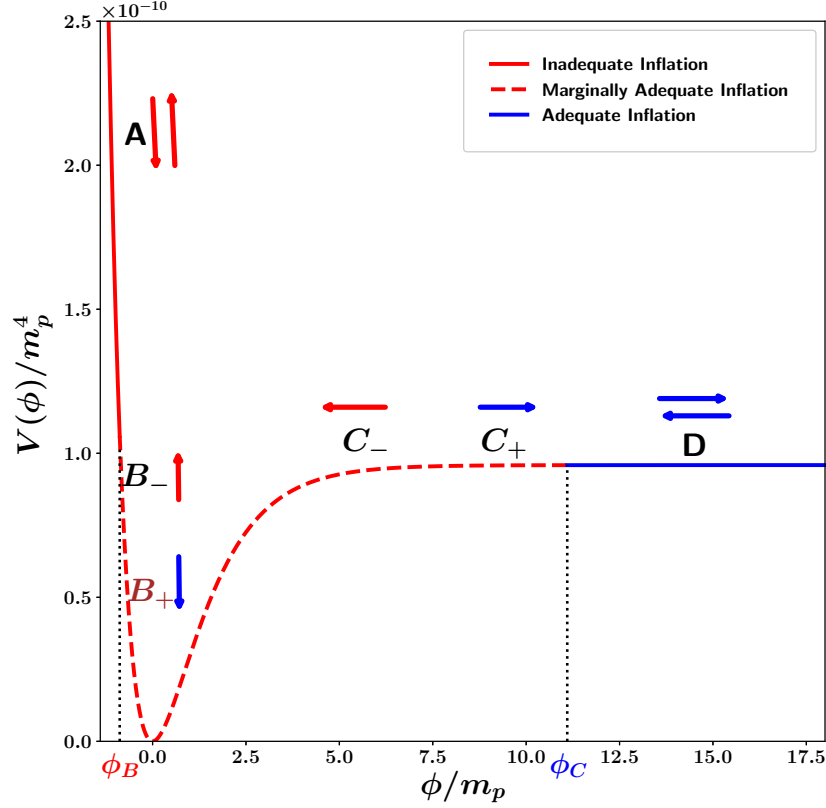


Figure 25: This figure schematically shows initial field values which lead to adequate and inadequate Starobinsky inflation. The initial energy scale is $H_i = 3 \times 10^{-3} m_p$. The solid blue line represents the region of adequate inflation while the solid red line displays the region of inadequate inflation. (Note that ϕ is unbounded on the right.) For initial field values lying in the interval $\phi_i \in [\phi_B, \phi_C]$ (red dashed line), one gets adequate inflation only if the initial velocity $\dot{\phi}_i$ is positive. This figure shows that it is easy for inflation to commence from the flat right wing of the potential. Note that only a small portion of the full potential is shown in this figure.

It may be noted that our results do not support some of the claims made in [12] that inflation in plateau-like potentials suffers from an *unlikeliness problem* since only a small range of initial field values leads to adequate inflation. The authors of [12] made this claim on the basis of a flat Mexican hat potential. Our analysis, based on more realistic models including Higgs inflation and Starobinsky inflation, has shown that, on the contrary, a fairly large range of initial field values (and initial energy scales) can give rise to adequate inflation, as illustrated in figures 18 and 25.

Finally we would like to draw attention to the fact that the phase-space analysis performed here for Starobinsky inflation is likely to carry over to the E-model α -attractor potential of loop quantum gravity.

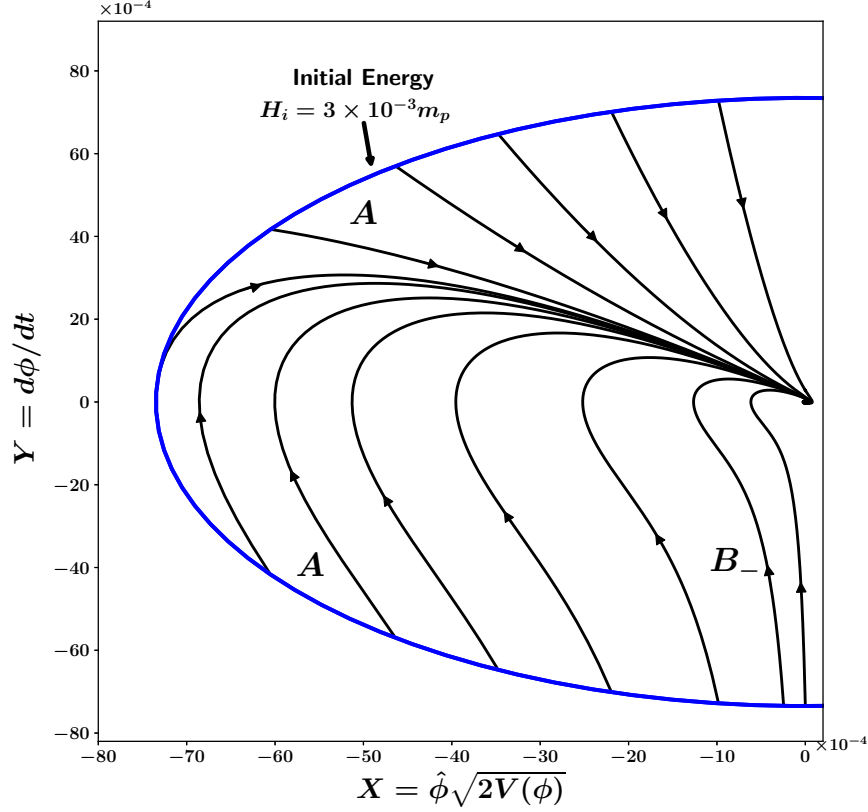


Figure 26: This figure illustrates the phase-space associated with the regions A and B_- on the steep left wing of the potential (5.3) illustrated in figure 25. As earlier, $Y = \dot{\phi}$ is plotted against $X = \hat{\phi} \sqrt{2V(\phi)}$ for the fixed initial energy scale $H_i = 3 \times 10^{-3} m_p$ (blue line). ($\hat{\phi} = \frac{\phi}{|\phi|}$ is the sign of field ϕ .) Note that the horizontal slow-roll inflationary separatrix is absent which reflects the fact that commencing from region A (and B_-) in figure 25, one cannot get adequate inflation from the steep left wing of the Starobinsky potential.

tential [34], since the two potentials are qualitatively very similar.

6 Discussion

In this paper we have addressed the issue of the robustness of inflation to different choices of initial conditions. We have widely varied the initial kinetic and potential terms $\frac{1}{2} \dot{\phi}_i^2$ and $V(\phi_i)$ for a given initial energy scale of inflation and determined the fraction of initial conditions which give rise to adequate inflation ($N_e \geq 60$). Our analysis has primarily focussed on the following models: (i) chaotic inflation and its extensions such as monodromy inflation, (ii) Higgs inflation, (iii) Starobinsky inflation. For class (i) we have shown that inflation becomes more robust for lower values of the exponent n in the inflaton potential $V \propto |\phi|^n$. This is illustrated in figure 13. Concerning (ii), it is well known that Higgs inflation can arise from a

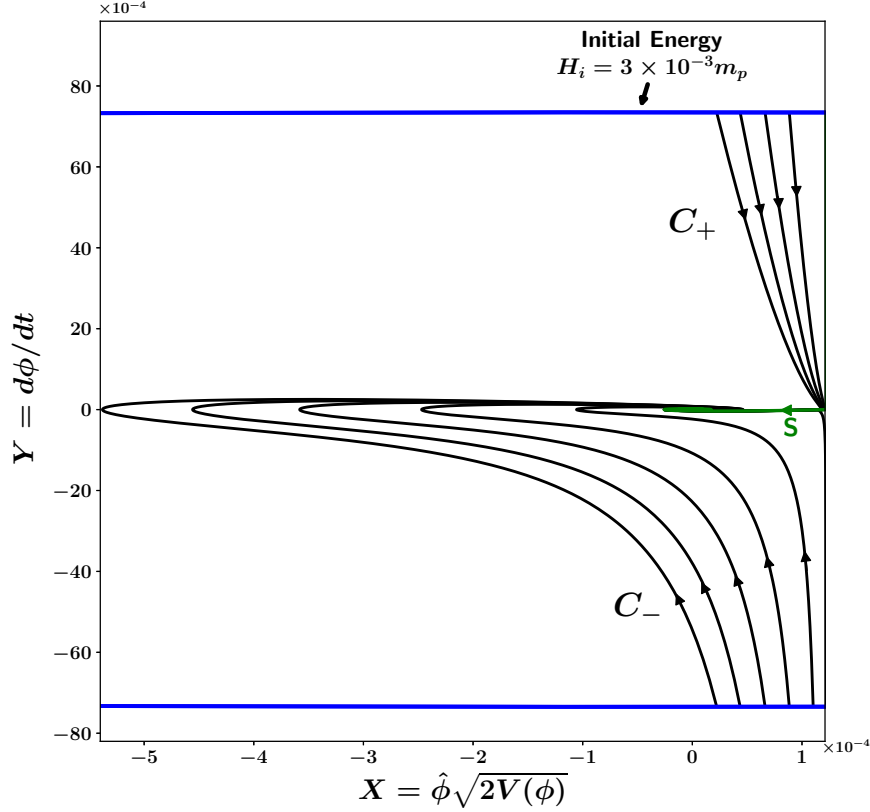


Figure 27: This figure illustrates the phase-space associated with the flat right wing of the potential (5.3). $Y = \dot{\phi}$ is plotted against $X = \hat{\phi}\sqrt{2V(\phi)}$ for the fixed initial energy scale $H_i = 3 \times 10^{-3}m_p$ (denoted by blue lines at the boundary). ($\hat{\phi} = \frac{\phi}{|\phi|}$ is the sign of field ϕ .) Note that trajectories commencing at the boundary with $\dot{\phi}_i > 0$ (region C_+ in figure 25) converge to the inflationary separatrix ‘S’ before winding up in spirals around the center (shown in detail in the next figure). By contrast, trajectories commencing on the right wing of $V(\phi)$ with $\dot{\phi}_i < 0$ in the region C_- in figure 25, do not lead to inflation.

non-minimal coupling of the Higgs field to the Ricci scalar. In this case the effective inflaton potential in the Einstein frame is asymptotically flat and has plateau-like features for large absolute values of the inflaton field. This is also true in the Einstein frame representation of the Starobinsky potential, but in this case one of the wings of $V(\phi)$ is flat while the other is steep (and cannot sustain inflation). A remarkable feature which is shared by (non-minimally coupled) Higgs inflation and Starobinsky inflation, is that one can get adequate inflation ($N_e \geq 60$) even if the inflaton commences to roll from the *minimum of the potential* ($\phi = 0$) and not from its periphery. This remarkable property is typical of asymptotically flat potentials and is not shared by the power law potentials commonly associated with chaotic

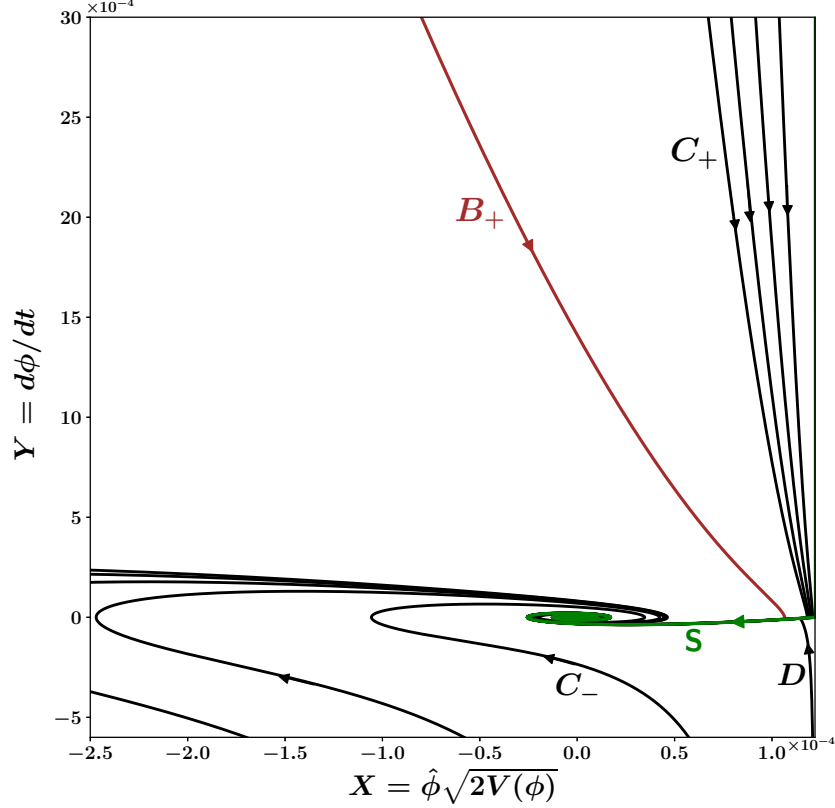


Figure 28: A zoomed-in view of the phase-space of Starobinsky inflation which highlights the existence of the slow-roll inflationary separatrix on the flat right wing (green line marked ‘S’ in figure 25). Most trajectories commencing on the right wing (from regions C_+ and D) converge to ‘S’ before spiralling in towards the minimum of $V(\phi)$. (The spirals correspond to post-inflationary oscillations.) Such an inflationary separatrix does not exist for the steep left wing of the potential. However note the brown trajectory which is able to meet the inflationary separatrix on the right wing even though it commences from region B_+ of $V(\phi)$ (but with $\dot{\phi}_i > 0$) as shown in figure 25. The brown trajectory describes the motion of the field ϕ as it rolls up the potential.

inflation. This new insight forms one of the central results of our paper.⁹

We also show that inflation can be sourced by a Higgs-like field provided the Higgs has a non-canonical kinetic term. In this case non-canonical inflation is more robust, and arises for a larger class of initial conditions, than canonical inflation.

Using phase space analysis we have shown that the fraction of trajectories which inflate *increases* with an increase in the value of the energy scale at which inflation commences. This

⁹Our results for Higgs and Starobinsky inflation are likely to carry over to the (α -attractor based) T-model [29] and E-model [34] respectively, due to the great similarity between the potentials of Higgs inflation and the T-model on the one hand, and Starobinsky inflation and the E-model on the other.

observation appears to be generic and applies to all of the models which have been studied in this paper.

One might note that our analysis in this paper assumes a specific measure on the space of initial conditions. Namely we assume that $X = \hat{\phi}\sqrt{2V(\phi)}$ ($\hat{\phi} = \frac{\phi}{|\phi|}$ is the sign of field ϕ) and $Y = \dot{\phi}$ are distributed uniformly at the boundary where initial conditions are set. Following this we determine the degree of inflation. While this approach follows the seminal work of [10], it is also possible to construct alternative measures. For instance one could assume instead that ϕ and $\dot{\phi}$ were distributed uniformly at the initial boundary. In this case the boundary will no more be a circle, as it was for chaotic inflation in figure 1. Instead its shape will crucially depend upon the form of $V(\phi)$. However we feel that as long as the initial phase-space distribution is not sharply peaked near specific values of $\phi_i, \dot{\phi}_i$, the broad results of our analysis will remain in place. (In other words we suspect that inflation is likely to remain generic for a large class of potentials, although we cannot prove this assertion.)

For the sake of simplicity we have confined our analysis of inflationary initial conditions to a spatially flat FRW universe. The reader is referred to [11, 35] for an early analysis of chaotic inflation in closed/open FRW universe models and to the more recent discussion in [36]. A discussion of inflation in homogeneous and anisotropic models can be found in [15].

7 Acknowledgements

A.V.T is supported by RSF Grant 16-12-10401 and by the Russian Government Program of Competitive Growth of Kazan Federal University. A.V.T is thankful to IUCAA, where this research work has been carried out, for the hospitality. S.S.M. thanks the Council of Scientific and Industrial Research (CSIR), India, for financial support as senior research fellow. S.S.M would also like to thank Surya Narayan Sahoo, Remya Nair and Prasun Dutta for technical help in generating some of the figures. S.S.M would like to thank Sanil Unnikrishnan for useful discussions and comments on the non-canonical Higgs inflation section.

A The values of n_s and r for several inflationary models

For single field slow-roll inflation, the amplitude of scalar fluctuations is given by [5]

$$\Delta_s^2 = \frac{1}{24\pi^2} \frac{V(\phi_*)}{m_p^4} \frac{1}{\epsilon(\phi_*)} \quad (\text{A.1})$$

where ϕ_* is the value of ϕ at N_e e-foldings before the end of inflation. CMB observations [16] imply $\Delta_s^2 = 2.2 \times 10^{-9}$ so that

$$\frac{1}{24\pi^2} \frac{V(\phi_*)}{m_p^4} \frac{1}{\epsilon(\phi_*)} = 2.2 \times 10^{-9} . \quad (\text{A.2})$$

Similarly, for single field slow-roll inflation, the scalar spectral index is given by [5]

$$n_s = 1 + 2\eta(\phi_*) - 6\epsilon(\phi_*), \quad (\text{A.3})$$

and the tensor to scalar ratio is given by [5]

$$r = 16\epsilon(\phi_*). \quad (\text{A.4})$$

Values of the CMB normalized parameters n_s and r for some of the inflationary models discussed in this paper are listed in table 7, assuming $N_e = 60$. The corresponding r vs n_s plot is shown in figure 29.

Model	$V(\phi)$	Parameter	n_s	r
Non-minimal Higgs	$V_0 \left(1 - e^{-\sqrt{\frac{2}{3}} \frac{ \phi }{m_p}} \right)^2$	$V_0 = 9.6 \times 10^{-11} m_p^4$	0.967	0.003
Starobinsky	$\frac{3}{4} m^2 m_p^2 \left(1 - e^{-\sqrt{\frac{2}{3}} \frac{\phi}{m_p}} \right)^2$	$m = 1.13 \times 10^{-5} m_p$	0.967	0.003
Fractional Monodromy	$V_0 \left \frac{\phi}{m_p} \right ^{2/3}$	$V_0 = 3.34 \times 10^{-10} m_p^4$	0.978	0.044
Linear Monodromy	$V_0 \left \frac{\phi}{m_p} \right $	$V_0 = 1.97 \times 10^{-10} m_p^4$	0.975	0.066
Quadratic Chaotic	$\frac{1}{2} m^2 \phi^2$	$m = 5.97 \times 10^{-6} m_p$	0.967	0.132
Quartic Chaotic	$\frac{\lambda_c}{4} \phi^4$	$\lambda_c = 1.43 \times 10^{-13}$	0.951	0.262

Table 7: This table lists the CMB normalized value of parameter, scalar spectral index n_s and tensor to scalar ratio r for different single field slow-roll inflationary models considered in this paper.

For Higgs inflation, substitution of the value $V_0 = 9.6 \times 10^{-11} m_p$ into equation (4.16), gives $\xi = 1.62 \times 10^4$ for the non-minimal coupling parameter, which is in agreement with equation (4.5).

B Jordan to Einstein frame transformation for Higgs inflation

A derivation of equations (4.10) and (4.11) is given below. Our derivation is similar to that given in [28], however we calculate the field transformation $\phi \rightarrow \chi$ explicitly. We commence with the Jordan frame action (4.1), namely

$$S_J = \int d^4x \sqrt{-g} \left[f(\phi) R - \frac{1}{2} g^{\mu\nu} \partial_\mu \phi \partial_\nu \phi - U(\phi) \right] \quad (\text{B.1})$$

which is described by the metric $g_{\mu\nu}$. The Einstein frame is described by $\hat{g}_{\mu\nu}$ where

$$\hat{g}_{\mu\nu} = \Omega^2 g_{\mu\nu} \quad (\text{B.2})$$

the conformal factor being given by

$$\Omega^2 = \frac{2}{m_p^2} f(\phi) = 1 + \frac{\xi \phi^2}{m_p^2}. \quad (\text{B.3})$$

Furthermore $\sqrt{-g}$ transforms as

$$\sqrt{-g} \rightarrow \sqrt{-\hat{g}} = \Omega^4 \sqrt{-g} \quad (\text{B.4})$$

and the Ricci scalar transforms as

$$R \rightarrow \hat{R} = \frac{1}{\Omega^2} \left[R - \frac{1}{\Omega} \square \Omega \right] \quad (\text{B.5})$$

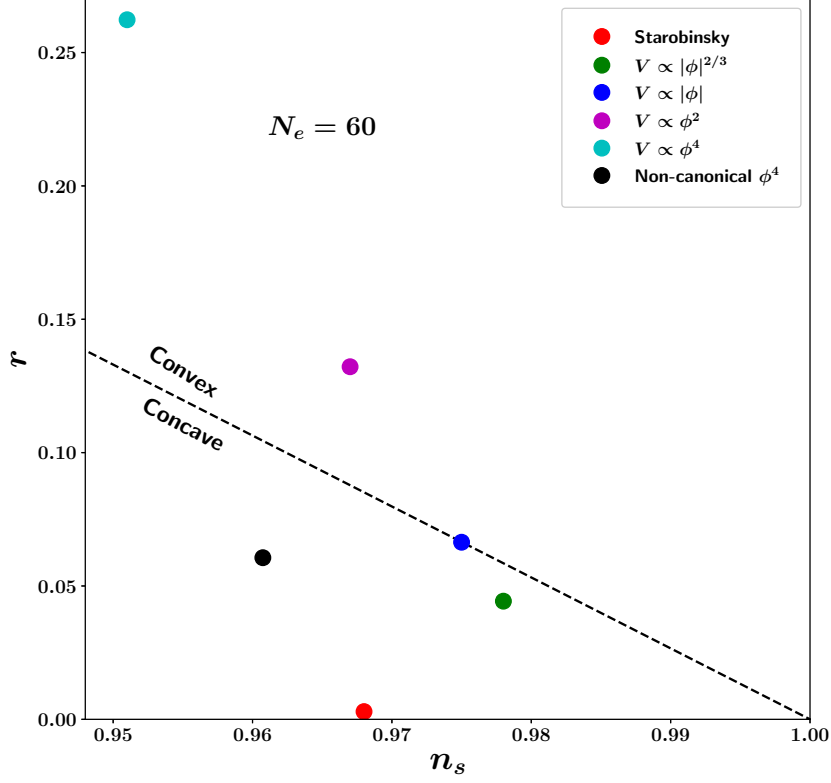


Figure 29: The values of tensor to scalar ratio r and the corresponding values of scalar spectral index n_s are plotted in this figure for different inflationary potentials considered in this paper corresponding to $N_e = 60$. Note that the values of r and n_s for the Starobinsky inflation (5.3) and the Higgs inflation in the non-minimal framework (4.15) are same since both the potentials have the same functional form as far as the flat inflationary wing is concerned. The value for the non-canonical $\lambda\phi^4$ potential has been determined assuming $\alpha = 5$ in (4.18).

where

$$\square\Omega = \frac{1}{\sqrt{-g}}\partial_\mu(\sqrt{-g}g^{\mu\nu}\partial_\nu\Omega).$$

As a result the action (B.1) transforms to

$$S = \int d^4x \sqrt{-\hat{g}} \left[\frac{m_p^2}{2} \hat{R} - \frac{1}{2} \hat{g}^{\mu\nu} \left(\frac{1}{\Omega^2} \partial_\mu \phi \partial_\nu \phi + \frac{6m_p^2}{\Omega^2} \partial_\mu \Omega \partial_\nu \Omega \right) - \frac{U(\phi)}{\Omega^4} \right]. \quad (\text{B.6})$$

Notice that the coupling of the scalar field to gravity has become minimal. However the kinetic term is non-canonical. In order to change this to the canonical form one redefines the

field $\phi \longrightarrow \chi$ such that

$$\frac{1}{2}\hat{g}^{\mu\nu}\left(\frac{1}{\Omega^2}\partial_\mu\phi\partial_\nu\phi + \frac{6m_p^2}{\Omega^2}\partial_\mu\Omega\partial_\nu\Omega\right) + \frac{U(\phi)}{\Omega^4} = \frac{1}{2}\hat{g}^{\mu\nu}\partial_\mu\chi\partial_\nu\chi + V(\chi) \quad (\text{B.7})$$

where

$$V(\chi) = \frac{U[\phi(\chi)]}{\Omega^4}. \quad (\text{B.8})$$

Consequently the action in the Einstein frame becomes

$$S_E = \int d^4x \sqrt{-\hat{g}} \left[\frac{m_p^2}{2} \hat{R} - \frac{1}{2} \hat{g}^{\mu\nu} \partial_\mu\chi\partial_\nu\chi - V(\chi) \right].$$

Note that assuming a homogeneous and isotropic space-time one can drop the spatial derivative terms in (B.7) to get

$$\begin{aligned} \frac{1}{\Omega^2} \left[\dot{\phi}^2 + 6m_p^2 \dot{\Omega}^2 \right] &= \dot{\chi}^2 \\ \Rightarrow \frac{1}{\Omega^2} \left[\dot{\phi}^2 + 6m_p^2 \left(\frac{\partial\Omega}{\partial\phi} \right)^2 \dot{\phi}^2 \right] &= \left(\frac{\partial\chi}{\partial\phi} \right)^2 \dot{\phi}^2 \\ \Rightarrow \left(\frac{\partial\chi}{\partial\phi} \right)^2 &= \frac{1}{\Omega^4} \left[\Omega^2 + \frac{6\xi^2\phi^2}{m_p^2} \right] \\ \Rightarrow \frac{\partial\chi}{\partial\phi} &= \pm \frac{1}{\Omega^2} \sqrt{\Omega^2 + \frac{6\xi^2\phi^2}{m_p^2}} \end{aligned}$$

which corresponds to (4.11). Note that the ' \pm ' sign here leads to the symmetric potential in figure 18.

C Derivation of asymptotic forms of the Higgs potential in the Einstein frame

Equations (4.11) and (B.8) can be rewritten as

$$\frac{\partial\chi}{\partial\phi} = \pm \frac{\sqrt{1 + \frac{\xi\phi^2}{m_p^2} + \frac{6\xi^2\phi^2}{m_p^2}}}{1 + \frac{\xi\phi^2}{m_p^2}} \quad (\text{C.1})$$

$$V(\phi) = \frac{U[\phi(\chi)]}{\Omega^4} \simeq \frac{\frac{\lambda}{4}\phi^4}{\left(1 + \frac{\xi\phi^2}{m_p^2}\right)^2}. \quad (\text{C.2})$$

Using these two equations we proceed to derive the following useful asymptotic formulae. ¹⁰

1. For $\phi \ll \sqrt{\frac{2}{3}} \frac{m_p}{\xi}$ one finds $\frac{\partial\chi}{\partial\phi} \simeq \pm 1$, consequently (C.2) simplifies to

$$V(\chi) \simeq \frac{\lambda}{4} \chi^4. \quad (\text{C.3})$$

¹⁰This analysis has been carried out assuming $\xi = 1.62 \times 10^4 \gg 1$.

2. For $\phi \gg \sqrt{\frac{2}{3}} \frac{m_p}{\xi}$ one finds $\frac{\partial \chi}{\partial \phi} \simeq \pm \frac{\sqrt{6} \frac{\xi \phi}{m_p}}{\Omega^2}$ where $\Omega^2 = 1 + \frac{\xi \phi^2}{m_p^2}$. Hence in this case

$$\chi \simeq \pm \sqrt{\frac{3}{2}} m_p \log \Omega^2(\phi). \quad (\text{C.4})$$

For $\sqrt{\frac{2}{3\xi^2}} \ll \frac{\phi}{m_p} \ll \frac{1}{\sqrt{\xi}}$, expression (C.4) reduces to

$$\chi \simeq \pm \sqrt{\frac{3}{2}} \frac{\xi \phi^2}{m_p}, \quad (\text{C.5})$$

consequently the potential in (C.2) acquires the form

$$V(\chi) \simeq \left(\frac{\lambda m_p^2}{6\xi^2} \right) \chi^2. \quad (\text{C.6})$$

Finally for $\frac{\sqrt{\xi} \phi}{m_p} \gg 1$ one finds, from (C.4)

$$\phi \simeq \frac{m_p}{\sqrt{\xi}} \exp \left(\frac{\pm \chi}{\sqrt{6} m_p} \right) \quad (\text{C.7})$$

where the '+' sign is taken for $\chi > 0$ and the '-' sign is taken for $\chi < 0$, since the above solution is valid only in the limit when $|\frac{\sqrt{\xi} \phi}{m_p}| \gg 1$. Consequently we can rewrite our solution as

$$\phi \simeq \frac{m_p}{\sqrt{\xi}} \exp \left(\frac{|\chi|}{\sqrt{6} m_p} \right), \quad (\text{C.8})$$

and the potential in (C.2) is given by

$$V(\chi) \simeq \frac{\lambda m_p^4}{4\xi^2} \left(1 + \exp \left[-\sqrt{\frac{2}{3}} \frac{|\chi|}{m_p} \right] \right)^{-2}. \quad (\text{C.9})$$

To summarize, the relation between χ and ϕ in the three asymptotic regions is given by

$$\frac{\chi}{m_p} = \begin{cases} \pm \frac{\phi}{m_p}, & \frac{\phi}{m_p} \ll \sqrt{\frac{2}{3\xi^2}}, \\ \pm \sqrt{\frac{3}{2}} \xi \left(\frac{\phi}{m_p} \right)^2, & \sqrt{\frac{2}{3\xi^2}} \ll \frac{\phi}{m_p} \ll \frac{1}{\sqrt{\xi}}, \\ \pm \sqrt{6} \log \left(\frac{\sqrt{\xi} \phi}{m_p} \right), & \frac{\phi}{m_p} \gg \frac{1}{\sqrt{\xi}} \end{cases}$$

References

- [1] A. A. Starobinsky, Phys. Lett. B **91**, 99-102 (1980).
- [2] A. H. Guth, Phys. Rev. D **23**, 347 (1981).
- [3] A. D. Linde, Phys. Lett. B **108**, 389 (1982).
- [4] A. Albrecht and P.J. Steinhardt, Phys. Rev. Lett. **48**, 1220 (1982).

- [5] A.D Linde, *Particle Physics and Inflationary Cosmology*, Harwood Academic (1990) [arXiv:hep-th/0503203]; A. R. Liddle and D.H. Lyth, *Cosmological Inflation and Large Scale Structure*, Cambridge University Press (2000); D. Baumann, TASI Lectures on Inflation, [arXiv:0907.5424].
- [6] V. F. Mukhanov and G. V. Chibisov, JETP Lett. **33**, 532 (1981).
- [7] S. W. Hawking, Phys. Lett. B **115**, 295 (1982).
- [8] A. A. Starobinsky, Phys. Lett. B **117**, 175 (1982).
- [9] A. H. Guth and S. -Y. Pi, Phys. Rev. Lett. **49**, 1110 (1982).
- [10] V. A. Belinsky, L. P. Grishchuk, I. M. Khalatnikov and Ya. B. Zeldovich, Phys. Lett. **155** B, 232 (1985).
- [11] V. A. Belinsky, H. Ishihara, I. M. Khalatnikov and H. Sato, Prog. Theor. Phys. **79**, 676 (1988).
- [12] A. Ijjas, P. J. Steinhardt and A. Loeb, Phys. Lett. B **723**, 261-266 (2013) [arXiv:1314.2785].
- [13] A. D. Linde, [arXiv:1710.04278].
- [14] S. Unnikrishnan, V. Sahni and A. Toporensky, JCAP **1208** (2012) 018 [arXiv:1205.0786].
- [15] R.M. Wald, Phys. Rev. D **28**, 2118 (1983); A.A. Starobinsky, JETP Lett. **37**, 66 (1983); I. Moss and V. Sahni, Phys. Lett. B **178**, 159 (1986); V. Sahni and L.A. Kofman, Phys. Lett. A **117**, 275 (1986); Phys.Lett. **A117**, 275 (1986); J.D. Barrow, Phys. Lett. B **180**, 335 (1986); J.D. Barrow, Phys. Lett. B **187**, 12 (1987); M. Mijic and J.A. Stein-Schabes, Phys. Lett. B **203**, 353 (1988); M. Mijic, M.S. Morris and Wai-Mo Suen, Phys. Rev. D **39**, 1496 (1989); K. Olive, Phys.Rept. **190**, 307 (1990); R.H. Brandenberger and J.H. Kung, Phys. Rev. D **42**, 1008 (1990); D.S. Goldwirth, Phys. Rev. D **43**, 3204 (1991); D.S. Goldwirth and T. Piran, Phys.Rept. **214**, 223 (1992); Y. Kitada and Kei-ichi Maeda, Class.Quant.Grav. **10**, 703 (1993); E. Calzetta and M. Sakellariadou, Phys. Rev. D **45**, 2802 (1992); R. Maartens, V. Sahni and T. D. Saini, Phys. Rev. D **63**, 063509 (2001) [arXiv:gr-qc/0011105]; C. Pitrou, T. S. Pereira and J.-P. Uzan, JCAP **0804** (2008) 004 [arXiv:0801.3596]; I. Ya. Aref'eva, N. V. Bulatov, L. V. Joukovskaya and S. Yu. Vernov, Phys. Rev. D **80**, 083532 (2009) [arXiv:0903.5264]; H.-C. Kim and M. Minamitsuji, Phys. Rev. D **81**, 083517 (2010), Erratum: Phys.Rev. D **82** (2010) 109904 [arXiv:1002.1361]; H.-C. Kim and M. Minamitsuji, JCAP **1103** (2011) 038 [arXiv:1101.0329]; S. Hervik, D. F. Mota and M. Thorsrud, JHEP **1111** (2011) 146 [arXiv:1109.3456]; A. Maleknejad, M.M. Sheikh-Jabbari and J. Soda, JCAP **1201** (2012) 016 [arXiv:1109.5573]; J. Soda, Class.Quant.Grav. **29** (2012) 083001 [arXiv:1201.6434]; A. Maleknejad and M.M. Sheikh-Jabbari, Phys. Rev. D **D85**, 123508 (2012) [arXiv:1203.0219]; A. Maleknejad and M.M. Sheikh-Jabbari, Phys.Rept. **528**, 161 (2013) [arXiv:1212.2921].
- [16] P. A. R. Ade et al. (Planck Collaboration), Planck 2015 results. XX., Constraints on Inflation, Astron. Astrophys. **594**, A20 [arXiv:1502.02114].
- [17] G N. Felder, A. V. Frolov, L. Koffinan and A.D Linde, Phys. Rev. D **66**, 023507 (2002) [arXiv:hep-th/0202017].
- [18] A. D. Linde, Phys. Lett. B **129**, 177 (1983).
- [19] A .D. Linde, Prog. Theor. Phys. Suppl. **163**, 295-322 (2006) [arXiv:hep-th/0503195].
- [20] E. Silverstein and A. Westphal, Phys. Rev. D **78**, 106003 (2008) [arXiv:0803.3085].
- [21] L. McAllister, E. Silverstein and A. Westphal, Phys. Rev. D **82**, 046003 (2010) [arXiv:0808.0706].
- [22] C. Germani and A. Kehagias, Phys. Rev. Lett. **105**, 011302 (2010); C. Germani and A. Kehagias, JCAP **05**(2010)019; C. Germani and A. Kehagias, Phys. Rev. Lett. **106**, 161302 (2011); C. Germani and Y. Yatanabe, JCAP **07**(2011) 031; S. Tsujikawa, Phys. Rev. D **85**, 083518 (2012).

- [23] F. L. Bezrukov and M. Shaposhnikov, Phys. Lett. B **659**, 703-706 (2008) [arXiv:0710.3755].
- [24] R. Fakir and W.G. Williams, Phys. Rev. D **41**, 1783-1791 (1990).
- [25] F. L. Bezrukov, D. Gorbunov and M. Shaposhnikov, JCAP 0906 (2009) 029 [arXiv:0812.3622].
- [26] J. Garca-Bellido, D. G. Figueroa, and J. Rubio, Phys. Rev. D **79**, 063531 (2009) [arXiv:0812.4624].
- [27] D. P. George, S. Mooij and M. Postma, JCAP, 1402 (2014) 024 [arXiv:1310.2157].
- [28] D. I. Kaiser, Phys. Rev. D **81**, 084044 (2010) [arXiv:1003.1159].
- [29] R. Kallosh and A. Linde, JCAP07 (2013) 002 [arXiv:1306.5220].
- [30] V. Mukhanov and A. Vikman, JCAP **0602**, 004 (2006) [arXiv:astro-ph/0512066].
- [31] K. I. Maeda, Phys. Rev. D **37**, 858 (1988).
- [32] D. S. Gorbunov and A. G. Panin, Phys. Lett. B **743**, 79-81 (2015) [arXiv:1412.3407].
- [33] B. Bonga and B. Gupt, Phys. Rev. D **93**, no.6, 063513 (2016) [arXiv:1510.04896].
- [34] R. Kallosh, A. Linde and D. Roest, JHEP11, 198 (2013) [arXiv:1311.0472].
- [35] V. A. Belinsky and I. M. Khalatnikov, Sov. Phys. JETP 66 (3) (1987).
- [36] A.H. Guth, D.I. Kaiser, Y. Nomura, Phys. Lett. B **733**, 112 (2014) [arXiv:1312.7619].